Chapter Two
An Overview of the Normal Stars

2.1 INTRODUCTION

Stellar spectra are astonishingly diverse. In the optical part of the spectrum, the vast majority are primarily absorption-line spectra, but even these range from the starkly simple A-type spectra, dominated by a few strong hydrogen lines, to the complex molecular spectra of M-type stars and carbon stars. For most stars, a solar mix of elemental abundances is a good first estimate, but there are some stars in which trace elements, such as the rare earths, or more common elements, such as carbon, are bizarrely enhanced. Some stars are hydrogen deficient, whereas others show marked underabundances of most metals. Certain stellar spectra, on the other hand, are dominated by emission lines. Wolf–Rayet stars, for example, show broad, strong emission lines in their spectra, clearly deriving from a massive stellar wind, whereas in the flare stars, common among the early M-type dwarfs, the emission lines are produced in active regions that might cover a significant fraction of the stellar surface.

This surprising diversity of spectral forms is a reflection of the wide range of physical phenomena that go into the formation of stellar spectra. It is remarkable, therefore, that the vast majority of stellar spectra can be comprehended on the basis of only two physical parameters—temperature and gas pressure (or its proxies, surface gravity and density). The purpose of this chapter is to take a first look at the variety of stellar types explained by those two physical parameters. First, we survey the two-dimensional array of *normal* stellar types from a descriptive, morphological point of view (the basis of the MK spectral classification system); second, we briefly examine an independent technique for classifying stars, i.e., multicolor photometry; and then, finally, we explore, using simple concepts from physics, how those two physical parameters can account for the observed array of spectral forms of normal stars.

2.2 THE SPECTRAL SEQUENCE

2.2.1 The Main Sequence

In Chapter 1 we traced the history of the MK spectral classification system, including the realization that the sequence of spectral types OBAFGKM represents a temperature sequence. That this ordering of spectral types is a temperature sequence is abundantly clear from Figure 2.1, which shows how the optical spectral

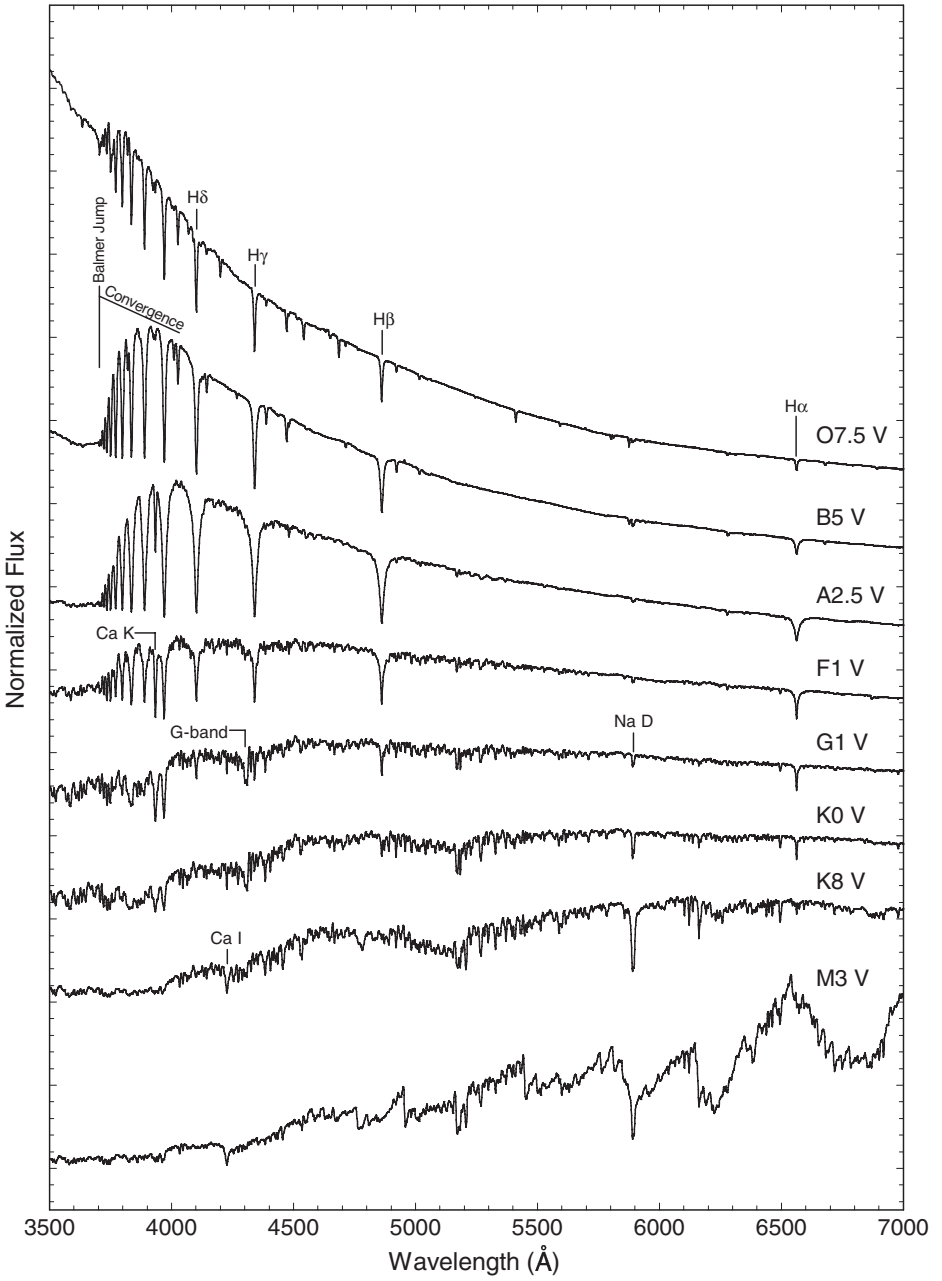

Figure 2.1 The OBAFGKM spectral sequence for main-sequence (dwarf) stars illustrating that the spectral sequence is ordered in terms of temperature. Here, the normalized stellar flux (the *energy distribution*) is plotted against wavelength. Some of the more prominent spectral features are marked, including the Balmer jump and convergence. The source of these spectra is the Indo-US coudé-feed spectral library (Valdes et al. 2004). The spectra have been normalized at a common wavelength, and separated by one continuum unit for clarity, except for the bottom spectrum, which is offset by 2 units.

energy distributions of main-sequence (*dwarf*[1]) stars vary with spectral type. This sequence is presented in more detail in Figures 2.2 and 2.3 in the blue-violet spectral region traditionally used for MK spectral classification. Figure 2.2 illustrates stars hotter than the Sun (these stars are commonly referred to as the *early-type stars*), and Figure 2.3 stars cooler than the Sun, the *late-type stars*. Note that these figures use two different spectral formats. In Figure 2.2 the spectra are presented in "rectified" format, in which the intensity of the continuum points (i.e., the points not affected by line absorption) has been normalized to unity. This is a convenient format to use as it permits the use of line ratios over a wide wavelength range in spectral classification. However, in the late-type stars, the density of the spectral lines is so great that there are no true continuum points, and so rectification of the spectrum is not the best representation. Instead, the most convenient format for these spectra in classification is the "normalized flux" format, in which the stellar fluxes have been normalized to unity at one common point. The spectra in Figure 2.3 have been normalized to unity at a common wavelength of 5445 Å.

A glance at Figure 2.2 indicates that the salient feature of the sequence of early-type spectra is the behavior of the hydrogen Balmer lines (the Hβ, Hγ, Hδ, Hϵ, H8, and H9 lines in the Balmer series are visible in these spectra). Note that in the O-type stars, the hottest normal stars, the Balmer lines (which in the O-type stars are actually blended with lines of the Pickering series of He II—see §2.4.2) are quite weak. With decreasing temperature (later spectral type), the Balmer lines increase in strength, coming to a maximum in the early A-type stars, at a spectral type of about A2. They then fade rapidly with decreasing temperature, and cease to dominate the blue-violet spectrum in K-type and later stars. In §2.4 we will use elementary concepts from atomic and statistical physics to understand this behavior. For the moment, it is sufficient to note that this behavior comes about through the interplay of the ionization and excitation of hydrogen.

Lines of other species show a similar behavior. For instance, lines of neutral helium (He I) are very weak in the early O-type stars, but grow in strength with decreasing temperature, coming to a maximum at a spectral type of B2 on the main sequence. They then fade and essentially disappear from classification–resolution spectra by A0. In the O-type stars, lines of singly ionized helium (He II) are already declining in strength; their peak would be attained only in stars substantially hotter than the hottest known O-type star.

Another outstanding feature of the spectral sequence is the appearance and rapidly growing strength of lines due to metals. While lines of doubly and triply[2] ionized metals appear in the spectra of the O-type stars, and singly and doubly ionized metals in the B-type stars, lines of metals begin to dominate the appearance of the blue-violet spectrum only in the A-type stars. The strongest metal line in this

[1]The terms *dwarf*, *giant*, and *supergiant* are commonly used to refer to stars that inhabit different parts of the *Hertzsprung–Russell diagram* (see Glossary). Stars on the main sequence are called dwarfs, whereas giants and supergiants have evolved off the main sequence.

[2]Notation such as Fe I, Fe II, Fe III, etc. is used to represent different ionization states of an atomic species. Thus, Fe I refers to neutral iron, Fe II to singly ionized iron (Fe^{+1}), Fe III to doubly ionized iron, etc.

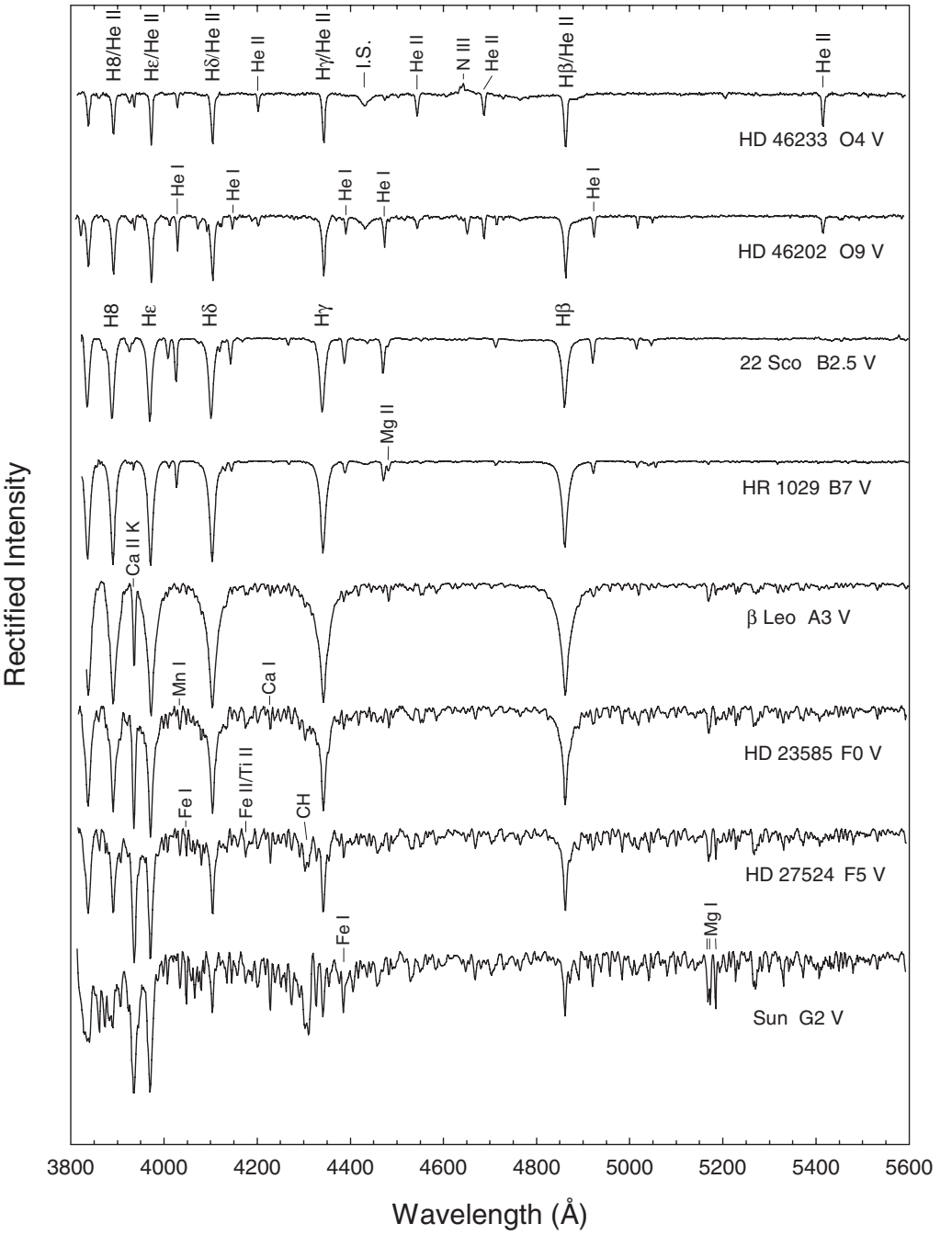

Figure 2.2 The Main Sequence from O4 to G2. Spectra in Figures 2.2–2.5 were obtained with the GM spectrograph on the 32″ telescope of the Dark Sky Observatory. These rectified spectra have a resolution of 3.6 Å, and have been offset by 0.7 continuum units for clarity.

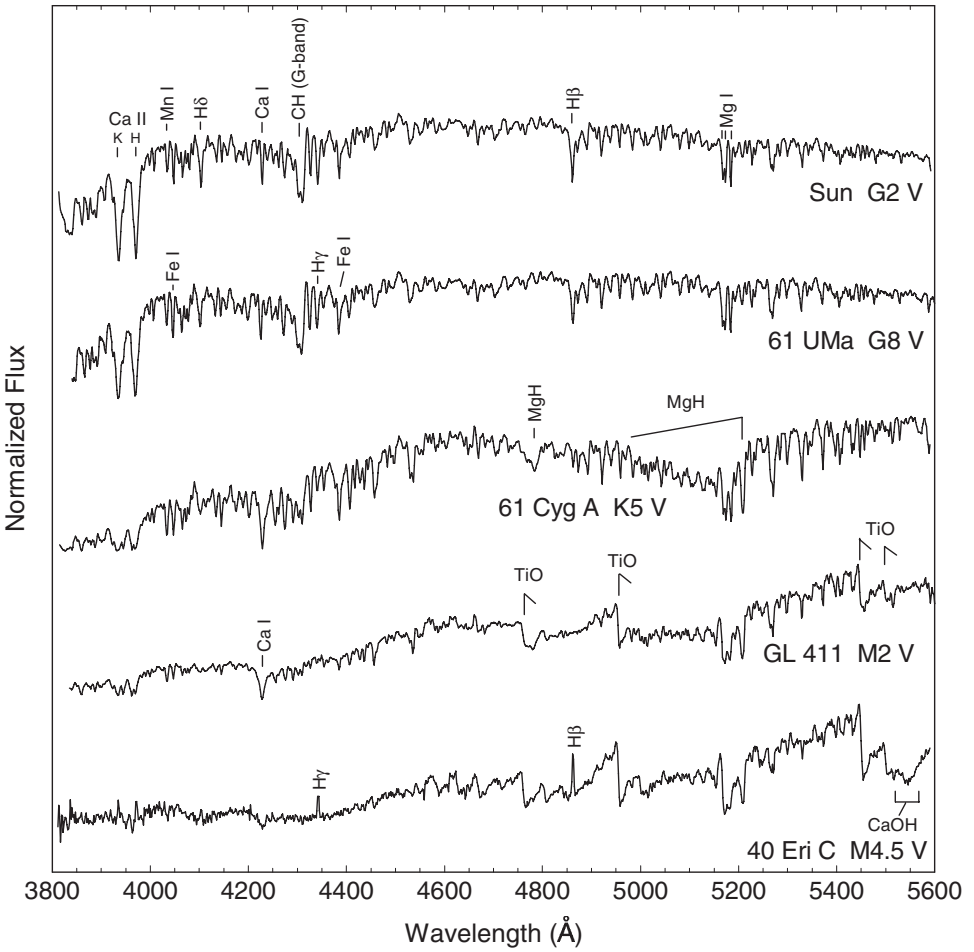

Figure 2.3 The Main Sequence from G2 to M4.5. These flux-calibrated spectra have been normalized at 5445 Å, and given integer vertical offsets for clarity.

spectral region, the Ca II K-line, first appears at a spectral type of B9 (some stars of earlier types show an interstellar Ca II K-line), and grows rapidly with decreasing temperature. Some of the metal lines commonly used in spectral classification are marked in Figures 2.2 and 2.3. Notice that most of these lines, especially the lines due to neutral species, grow in strength with decreasing temperature until a spectral type of K5, after which many begin to decline in strength. While this behavior appears superficially like that of the hydrogen and helium lines, the physics governing these line strengths is considerably more complex. We will consider this physics in more detail in §2.4.

Finally, spectral features due to molecules make their first appearance in the early F-type stars. The feature marked "CH" in the F5 star in Figure 2.2 is due to the diatomic molecule CH and is called the G-band. This molecular band grows rapidly in strength and comes to a maximum in the dwarfs at a spectral type of K2,

after which it fades away. In the K-type stars, molecular bands due to CN and MgH are prominent in the blue-violet region. The M-type spectra are dominated by strong bands of TiO. In even later spectra (as we will see in Chapters 8, 9 and 10), and in spectra of stars with unusual abundances (see, for instance, Chapter 8), many other molecules make their appearance, including polyatomic molecules. Note the band due to CaOH in the M4.5 dwarf in Figure 2.3.

2.2.2 Supergiants

Figures 2.4 and 2.5 present similar sequences for Ib supergiant stars and can be compared directly with Figures 2.2 and 2.3 for the dwarfs. Note that superficially the sequences appear very similar. However, there are a number of important differences. Consider the Balmer lines. In the supergiants, we see a behavior similar to what we saw in the dwarfs; the Balmer lines are weak in the O-type stars, come to a maximum in the A-type stars, and then fade for later spectral types. However, the details are different. Notice that for the early-type stars the Balmer lines are broader in the dwarfs than in the supergiants, and that in the supergiants the maximum occurs at a later spectral type. For instance, in the dwarfs the maximum in the Balmer lines occurs at a spectral type of A2; in the Ib supergiants the maximum is in the late A-type stars, or even at F0. Later than F0 the Balmer lines in the dwarfs and supergiants have essentially the same strengths.

In the A-, F-, and G-type supergiants, the metal lines are, with few exceptions, considerably stronger than the same lines in the dwarfs. This is particularly true for lines of ionized metals; some prominent lines and blends of lines of ionized metals that have significantly different strengths in the dwarfs and supergiants are marked in Figure 2.4.

In the late-type supergiants (Figure 2.5) note the strong CN band in 9 Peg, the G5 Ib standard, and its absence in the G-dwarfs (Figure 2.3). In addition, in the K5 dwarf in Figure 2.3, two molecular bands due to MgH are prominent, whereas these spectral features are weak or absent in the supergiants.

These differences (and others) in the spectra of main-sequence and evolved stars can be exploited in *luminosity classification*. A brief overview of luminosity classification is given in §2.2.4, but the details are best left for later chapters.

2.2.3 Sequences in the Ultraviolet and Infrared

2.2.3.1 The Ultraviolet

Ideally, a star should be classified in the region of the spectrum where its energy distribution peaks. Thus, the hot O- and B-type stars are ideally classified in the ultraviolet, A- through K-type stars in the optical, and M-type and later objects in the red and infrared. Of course, for ground-based telescopes, the ultraviolet and much of the infrared are inaccessible, a fact that in the past dictated that spectral classification was carried out largely in the optical. Other considerations may also require that stars be classified in spectral regions far from their flux peak. For instance,

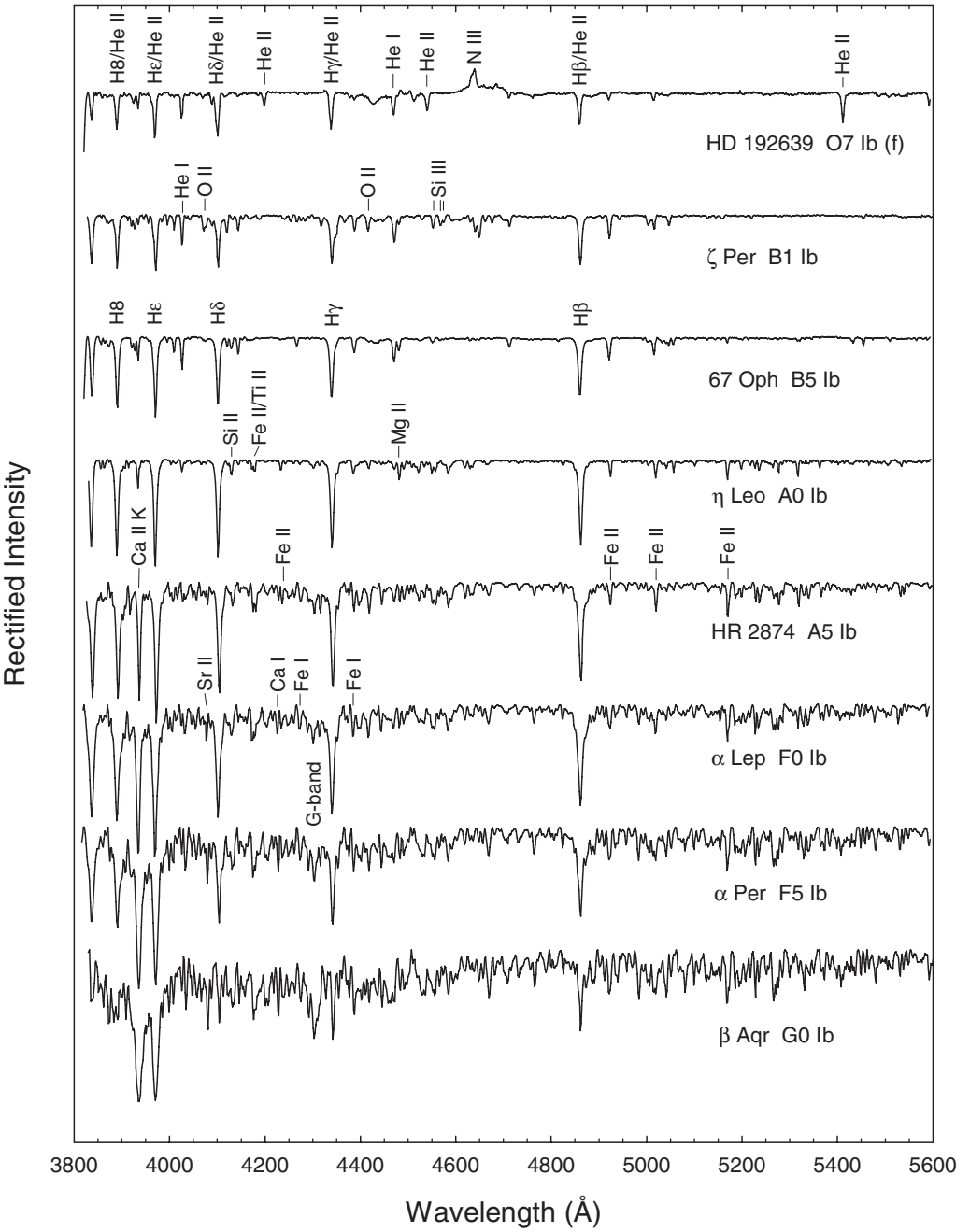

Figure 2.4 Ib Supergiants from O7 to G0. These spectra are rectified, and have been offset vertically by 0.7 continuum units.

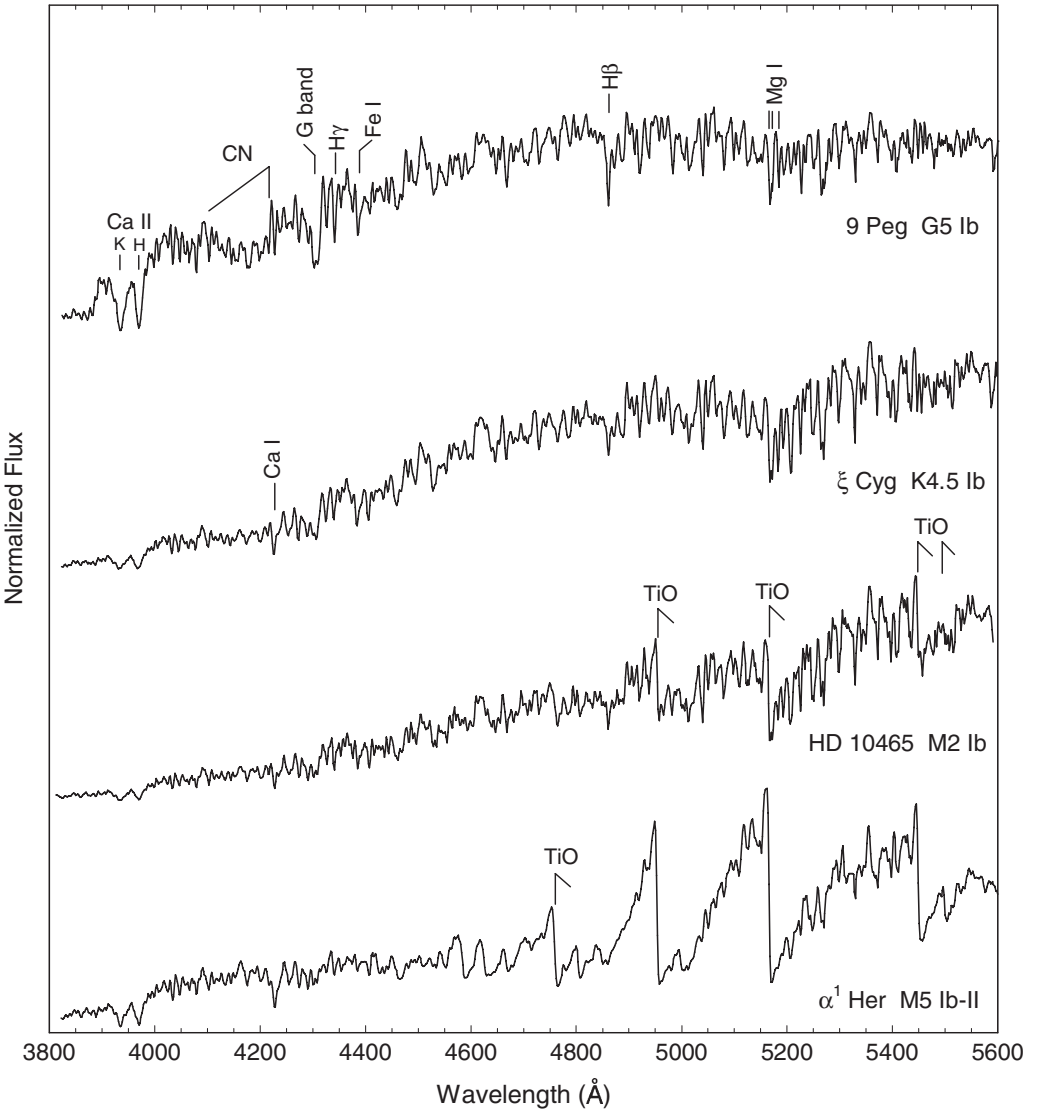

Figure 2.5 Ib Supergiants from G5 to M5. These spectra are in normalized flux format, and have been given integer vertical offsets for clarity.

in star-formation regions, the presence of dust may cause such large extinctions in the ultraviolet and optical that observations in those spectral regions are impossible. In such circumstances, observing and classifying O- and B-type stars in the infrared may be the only option. We will consider one such classification system for the O- and B-type stars in Chapter 3.

Figures 2.6 and 2.7 show spectral sequences for main-sequence stars in the ultraviolet and in the H-band region ($\approx$1.65 μm) of the infrared. The ultraviolet montage is based on spectra obtained with the International Ultraviolet Explorer

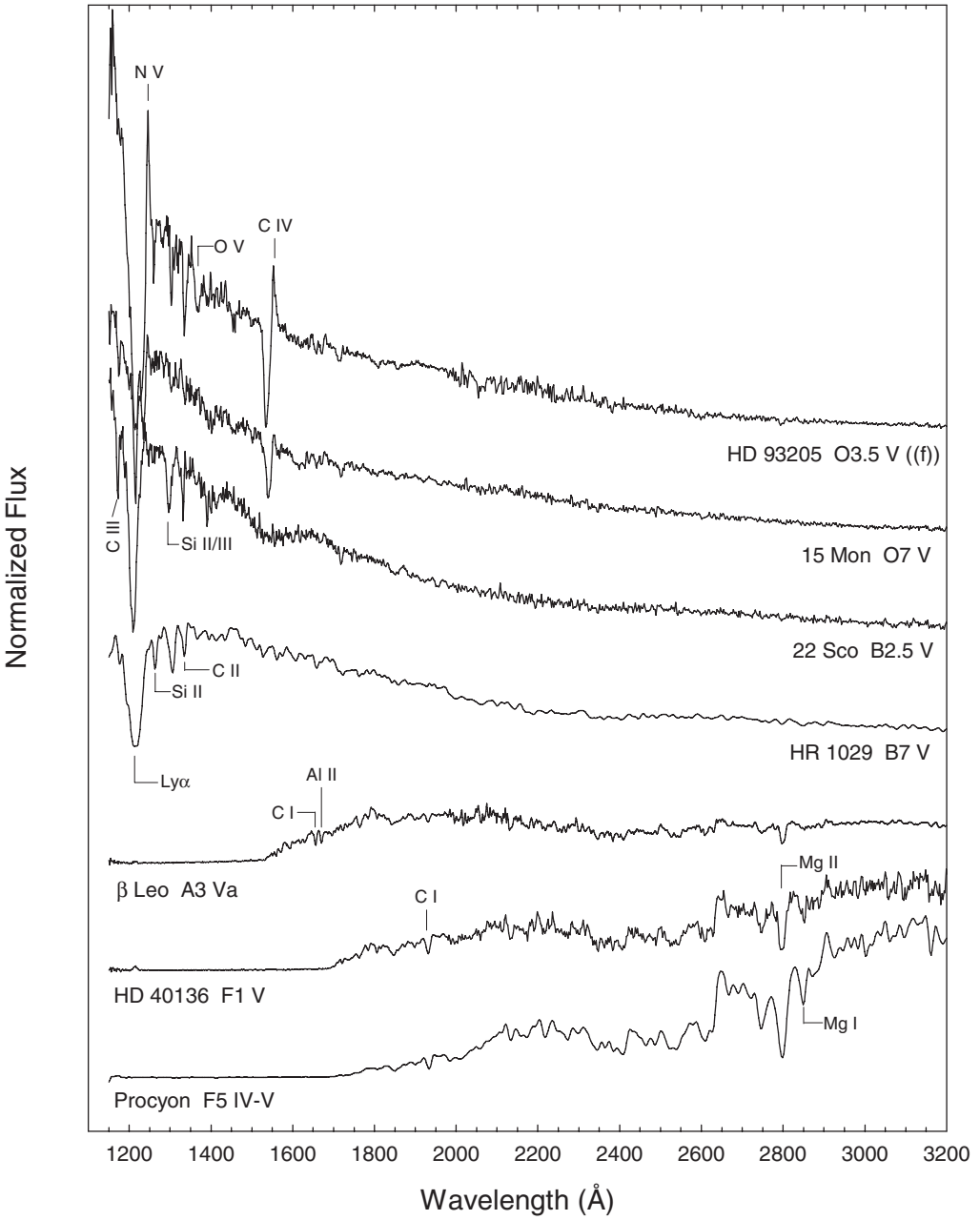

Figure 2.6 The Main Sequence in the ultraviolet. The spectra in this figure are from the International Ultraviolet Explorer data archives (MAST IUE http://archive.stsci.edu/iue). The spectra for both HD 93205 and 15 Mon have been dereddened. These spectra have been normalized at a common wavelength and given integer vertical offsets.

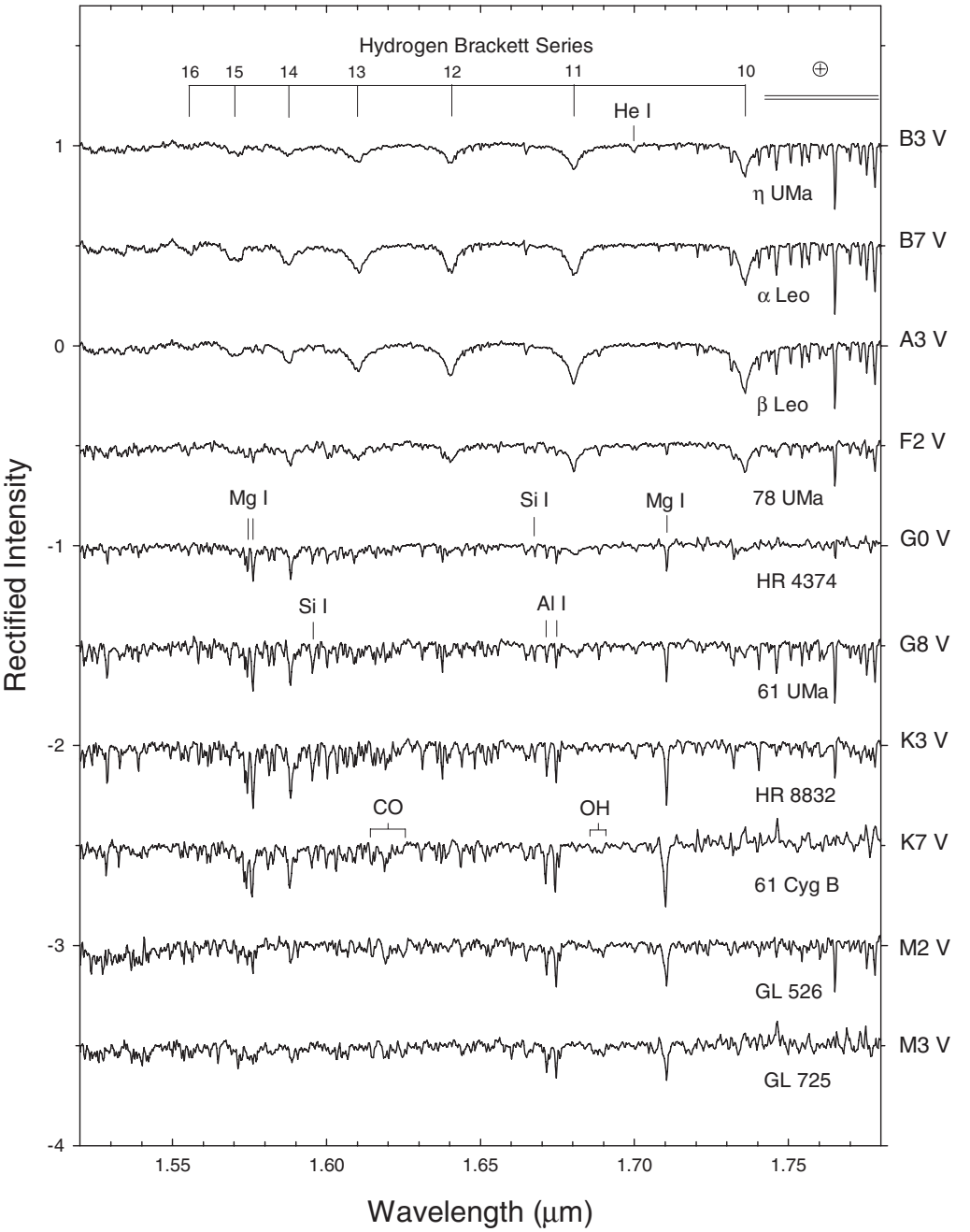

Figure 2.7 The Main Sequence in the H-band infrared. The spectra in this figure are from Meyer et al. (1998) and have been rectified. They have been given half-integer vertical offsets.

spacecraft (IUE) in the low dispersion mode. The infrared sequence is based on spectra obtained by Meyer et al. (1998). In the ultraviolet sequence, we have displayed the spectra in the normalized flux format to illustrate the enormous change in the ultraviolet flux as the temperature decreases. For stars much cooler than the Sun, the photospheric contribution to the ultraviolet region is minimal and instead this region is dominated by chromospheric and coronal emission lines. The strengths of these emission lines depend strongly on factors other than temperature and gravity (for instance, rotation and magnetic field strength), and thus cannot be used in a spectral classification system organized according to temperature and luminosity.

In Chapters 3 and 4 we will consider spectral classification systems for the O- and B-type stars based on high-resolution ultraviolet spectra. Figure 2.6 uses low-resolution IUE spectra, with a resolution of only about 6–9 Å. Even at such a low resolution features useful for spectral classification are visible. Notice in the O3.5 V spectrum the presence of strong lines due to highly ionized species (N V, Fe V, O V, C IV). The C IV feature exhibits a P Cygni profile consisting of a strong, blue-shifted absorption component combined with an emission component. This profile is the signature of a stellar wind; the absorption component is formed in the cylinder of expanding gas that we see in front of the stellar disk and the emission component from the remainder of the expanding shell (see Figure G.2). A similar profile can be seen for the N V line. While nearly all classes of stars have stellar winds, the mass-loss rates decline precipitously along the main sequence, and thus spectral wind features tend to fade toward later types.

The strongest line in the B-type stars in the ultraviolet region is the hydrogen Lyman-α line (1216 Å). Other lines in the Lyman series lie outside of the IUE spectral range but have been observed with the FUSE satellite (see Chapters 3 and 11). It is of interest to note that no lines of He I appear in the IUE spectral range. Lines of ionized helium do appear in this region, but are generally weak and not easily discerned at low resolution.

As we proceed toward cooler types in Figure 2.6, the flux in the far (shortwave) ultraviolet becomes less dominant, and the species that form the strongest lines tend to be in lower ionization states. In the A- and F-type stars, the shortwave ultraviolet vanishes. This is partly a consequence of the cooler temperatures of these stars, but also caused by the presence of both strong continuous and line absorption due to metals (see §2.4) in the atmospheres of these stars. A prominent feature that grows rapidly with declining temperature in the A- and F-type stars is the Mg II line (actually a blend of two strong lines, the Mg II h and k lines). These lines arise from energy levels analogous to those in the Ca II ion that give rise to the Ca II H and K lines and thus behave in a similar way.

2.2.3.2 The Infrared

The infrared is traditionally divided into a number spectral regions accessible from the ground through atmospheric "windows." The regions or "bands" most often

utilized for stellar spectroscopy include the J-band ($\approx$1.24 μm), the H-band ($\approx$1.65 μm), the K-band ($\approx$2.2 μm) and the L-band ($\approx$3.4 μm). Other regions in the infrared tend to have too much telluric (terrestrial atmospheric) absorption to make ground-based spectroscopy practical, and thus can be exploited only by space-based instruments (see §13.3).

For pedagogical purposes we will confine our discussion of the infrared in this chapter to the H-band sequence of main-sequence stars presented in Figure 2.7. Detailed spectral sequences in the J-, H-, K-, and L-bands for the different spectral types will be presented in later chapters.

The spectra of early-type stars in the H-band are dominated by lines of hydrogen. In the H-band, these hydrogen lines are members of the Brackett series (which arise from transitions out of the $n = 4$ energy level; the Balmer series, which is visible in the optical and near ultraviolet, arises from transitions out the $n = 2$ energy level in the hydrogen atom). Only the higher lines in the Brackett series are visible here; Brackett-α lies at about 4 μm and Brackett-γ is in the K-band. The designation we will use in this book for hydrogen (and He II) lines higher than ϵ in a series is the principal quantum number of the upper energy level of the transition. Thus, Balmer H8 arises from the transition $2 \rightarrow 8$, Brackett-10 from the transition $4 \rightarrow 10$.

The behavior of these hydrogen lines is quite similar to that of the Balmer lines in the optical; the hydrogen lines are relatively weak in the hottest stars, come to a maximum at an intermediate temperature, and then fade in the F- and G-type stars. A comparison with Figure 2.2, however, shows a subtle difference. In the optical, the hydrogen lines come to a maximum at A2 in the dwarf stars. In the H-band we see that B7 and A3 stars have hydrogen-line strengths that are nearly identical, implying that the maximum lies closer to A0, and may even be in the late B-type dwarfs. This difference is easily understood on the basis that the Brackett lines arise from a higher level in the hydrogen atom than the Balmer lines, as we will see in §2.4.

Other features show behaviors similar to the optical. Lines due to neutral metals gradually strengthen as we go toward later types, and come to a maximum at a spectral type of about K7, after which they tend to fade. Molecular absorption is less important in the H-band than in the optical, however. The prominent TiO bands that dominate the spectra of M-dwarfs in the optical extend only to about 1 μm, and thus do not contribute to the H-band. The only molecules that show absorption features strong enough to be easily visible in these H-band spectra are CO and OH.

2.2.4 Luminosity Classification

The MK System is fundamentally a two-dimensional system, consisting of a temperature dimension (*the spectral sequence*), which we considered in outline in the previous sections, and a luminosity dimension, which separates dwarfs (main-sequence stars) from evolved stars. Table 2.1 lists the main luminosity classes

Table 2.1 Luminosity Class (L.C.) Notation

L.C.	Name	L.C.	name
V	dwarf	Ib	supergiant
IV	subgiant	Ia	bright supergiant
III	giant	0	hypergiant
II	bright giant		

employed in the MK System, but be aware that subdivisions (such as IV–V) are commonly employed, and that the notation for these subdivisions can vary from one spectral class to the next, mostly for historical reasons. The luminosity class VI has been used historically to classify stars that lie below the main sequence in luminosity (i.e., the so-called *subdwarfs*) but this notation is no longer commonly employed (for exceptions see Chapters 4, 9, and 10).

Luminosity classification is carried out using spectral criteria that are peculiar to the spectral class, and even, in some cases, spectral subclass, and thus the details of luminosity classification are best left to the later chapters that are devoted to the individual spectral classes.

However, to establish some terminology, let us consider two specific examples. If a spectral feature strengthens with increasing luminosity (i.e., if it strengthens along the sequence V $\rightarrow$ III $\rightarrow$ I), then we say that it exhibits a *positive luminosity effect*. On the other hand, if it weakens along the same sequence, we say that it exhibits a *negative luminosity effect*. The hydrogen lines in the early A-type stars exhibit a negative luminosity effect. Compare the width of the hydrogen lines in the A3 V star in Figure 2.2 with the hydrogen lines of the supergiant A0 and A5 stars in Figure 2.4. The marked narrowing of the hydrogen lines with increasing luminosity in the early A-type stars can be used as a sensitive luminosity criterion. On the other hand, lines of Fe II and Ti II in the F-type stars tend to increase in strength with increasing luminosity. For instance, compare the Fe II/Ti II feature at $\lambda\lambda$4172–8 marked in the dwarf sequence in Figure 2.2 with the same feature in the supergiants in Figure 2.4. This is an example of a luminosity criterion that exhibits a positive luminosity effect.

2.3 MULTICOLOR PHOTOMETRY AND STELLAR CLASSIFICATION

In the previous section, we reviewed the outline of stellar spectral classification. The rest of the book will fill in the details! It should be noted at this point, however, that stellar classification may be carried out using techniques other than spectroscopy. In particular, stars may be classified, or at least characterized, with multicolor photometry. There are many existing systems of multicolor photometry, but all have in common the use of measurements of stellar brightnesses or *fluxes* in certain spectral bands. The isolation of the stellar bands is usually accomplished with glass and/or interference filters, and the flux measurements, traditionally obtained with photomultipliers, are now increasingly being acquired with CCDs.

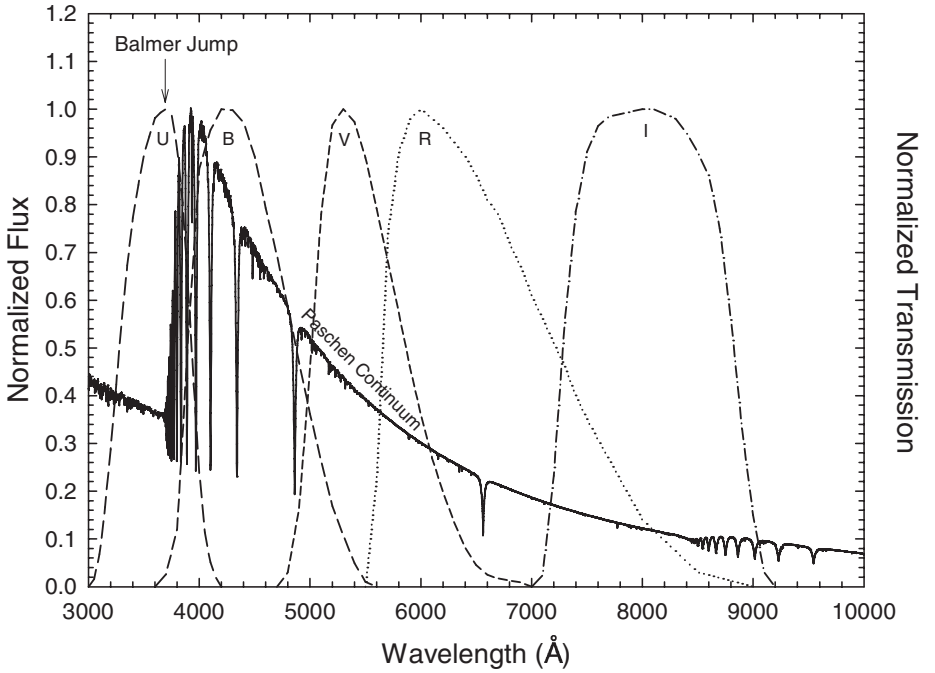

Figure 2.8 The normalized Johnson–Cousins $UBVRI$ photometric passbands (right-hand scale) plotted with the spectral energy distribution of an A0 V star (left-hand scale). The stellar energy distribution has been normalized to unity at the highest point. Notice the positions of the Balmer jump and the Paschen continuum. The Balmer lines are easily visible, and converge at a wavelength of 3646 Å. The scale of the right-hand vertical axis is identical to the left.

Multicolor photometry has a long and interesting history, but even a precis of that history is beyond the scope of this book. Interested readers are referred to the book *The Measurement of Starlight: Two Centuries of Astronomical Photometry* by Hearnshaw (2005). In the modern era, the most widely used, although not necessarily the best designed, photometric system is the Johnson *UBV* system (Johnson & Morgan 1953). Figure 2.8 shows the stellar energy distribution (flux spectrum) of an A0 V star plotted with the transmission passbands of the U (ultraviolet), B (blue), and V ("visual" or yellow-green) filters. In normal practice, stellar fluxes measured through these filters are converted to magnitudes, and placed on the standard *UBV* system via observations of standard stars. These magnitudes may be used to form the *photometric indices* $U{-}B$ and $B{-}V$. The $B{-}V$ index (or color) is a measure of the slope of the Paschen continuum (see Figure 2.8), and as such is quite closely correlated with the *effective temperature* of the star, although dwarfs and giants must be considered separately, and metal-weak stars do not obey the same relation as metal-rich. The $U{-}B$ index is also related to temperature, and is especially useful in the early-type stars for that purpose, but it is sensitive to other factors as well. Figure 2.8 shows that the U and B filters span and overlap the *Balmer jump*, a spectral discontinuity caused by the

photoionization of hydrogen from the first excited level ($n = 2$; see §2.4 and the discussion of *continuous opacity*), and the convergence of the Balmer series of hydrogen lines. The "height" of the Balmer jump is primarily sensitive to temperature in the early-type stars, but also shows significant sensitivity to pressure (surface gravity) in the A- and F-type stars, and thus $U-B$ is sensitive to both temperature and gravity. But, because the density of spectral lines due to metals is greater shortwards of the Balmer jump than longwards, the $U-B$ index is also sensitive to the overall metal abundance (sometimes called *metallicity*). Combine these various sensitivities with the fact that the short-wavelength cutoff of the U-filter passband is actually set by atmospheric absorption, and it is not surprising that the $U-B$ index can be difficult to interpret and model astrophysically.

UBV photometry is quite often combined with photometry in two other filters in the red and near-infrared, the R and I filters. Figure 2.8 shows the passbands of the R and I filters on the Johnson–Cousins system, which are quite different from the passbands of the R and I filters on the Johnson system. Users of photometry published in the literature must be careful to ascertain which passbands were employed. The Johnson–Cousins system has been carefully standardized by Arlo Landolt (see, for instance, Landolt 1992).

Another commonly used multicolor photometric system is the Strömgren $uvby$ system, designed by Bengt Strömgren in the 1960s (see Strömgren 1966). This system employs filters with narrower passbands than the Johnson *UBV* system; this enables the color indices on this system to be more easily interpreted astrophysically. Figure 2.9 plots the passbands of the four Strömgren filters with the energy distribution of an A0 V star. Notice that the u (ultraviolet) and v (violet) filters are more intelligently placed with respect to the Balmer jump and convergence than in the *UBV* system, although the Hδ line lies within the passband of the v filter. The $b-y$ index measures, like the B–V index on the Johnson system, the slope of the Paschen continuum. Two other indices are defined in the Strömgren system. The m_1 index, defined by $m_1 = (v-b) - (b-y)$, was designed to measure the *line blanketing* (absorption by spectral lines) in the v band; the $(b-y)$ term in the definition of the m_1 index helps to remove, to first order, the temperature sensitivity of this index. The c_1 index, defined by $c_1 = (u-v) - (v-b)$, measures the height of the Balmer jump, and is relatively free of the photometric effects of the Balmer convergence, unlike the $U-B$ index. In addition, the $(v-b)$ term in the definition of the c_1 index removes, to first order, the metallicity sensitivity of that index. The c_1 index comes to a maximum in the early A-type stars, like the hydrogen Balmer lines (see §2.2 and Figure 2.10). Strömgren photometry was designed explicitly for the detection and study of metal-weak F- and G-type stars, but has also found applications in the B-, A-, K-, and M-type stars (see, for instance Crawford 1975, 1978, 1979; Olsen 1983; Olsen & Perry 1984; Olsen 1995).

Strömgren $uvby$ photometry is often used with Hβ photometry, which consists of two filters centered on the hydrogen (Balmer) β line. One filter is narrow (full-width $\approx$60 Å), the other is wider (full-width $\approx$300 Å; see Crawford & Mander 1966). The inclusion of Hβ photometry helps in the determination of interstellar reddening.

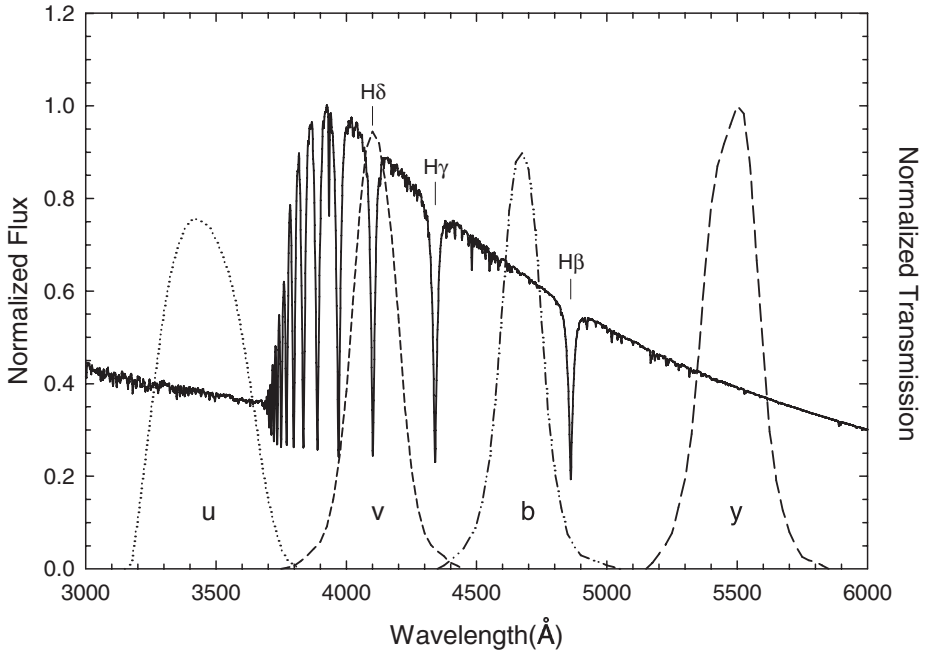

Figure 2.9 The Strömgren $uvby$ photometric passbands (right) plotted with the spectral energy distribution of an A0 V star (left). Notice that the narrower bands of the Strömgren system more cleanly sample the Balmer jump than the Johnson *UBV* passbands. The Strömgren passbands in this figure have been normalized to the peak transmission of the y band. The scales of the two vertical axes are identical.

A more recent photometric system, combining some of the filter passbands of the Strömgren system with those of the Vilnius system, has been developed, largely through the efforts of Straižys and colleagues (Straižys et al. 1996). This new system is called Strömvil photometry, and time will tell whether it will be widely adopted. Another photometric system that has similar properties to the Strömgren system is Geneva photometry (see, for instance, Nicolet 1996).

Yet another recently developed photometric system is the $u'g'r'i'z'$ Sloan Digital Sky Survey (SDSS) photometric system. The sixth release of data from the SDSS contains photometry of 287 million unique objects, including stars and galaxies. Table 2.2 lists the effective wavelengths of the five Sloan filters. For more information on the survey and $u'g'r'i'z'$ photometry, see `http://www.sdss.org`.

Over the years a large number of photometric systems have been developed, often for special purposes. It is beyond the scope of this book to review these systems, but the following merit mention: the DDO system for the measurement of red giants, incorporating filters to sample the CN molecular bands (McClure 1976); the Wing narrow-band system for late-type stars (White & Wing 1978); and the Washington system for late-type stars (Canterna 1976). Photometric systems have also been defined for the ultraviolet and infrared, such as the 2MASS JHK infrared photometric system (Skrutskie et al. 2006).

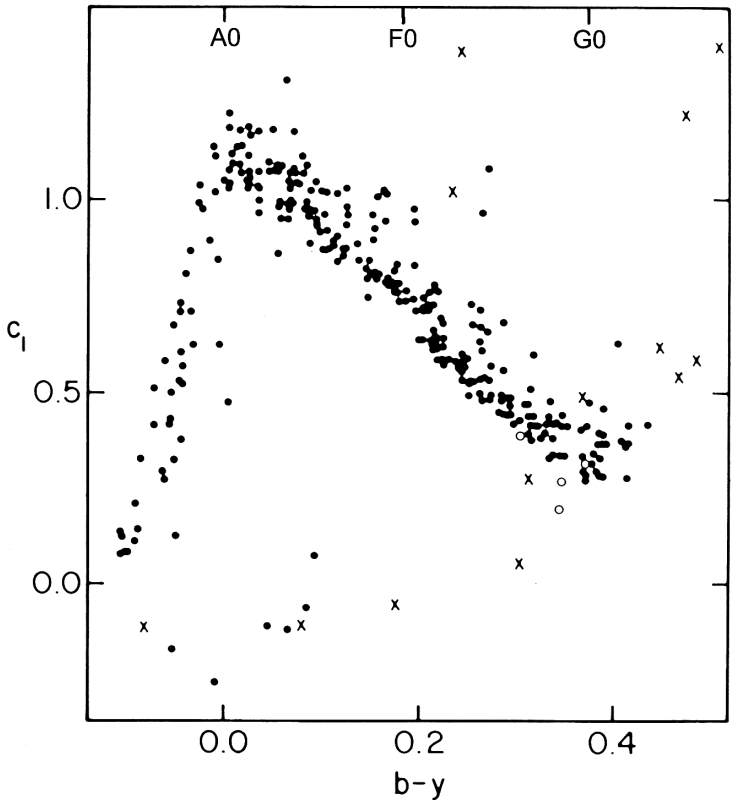

Figure 2.10 The $b-y$ index plotted against the c_1 index for the bright stars. Both indices are on the Strömgren $uvby$ photometric system. The $b-y$ index, in the absence of reddening, measures the temperature, the c_1 index, the Balmer jump. Note that the c_1 index comes to a maximum near $b-y = 0.0$, corresponding to the early A-type stars. The approximate positions of main-sequence spectral types have been added to the top scale for reference purposes. Figure from Crawford (1984) and used with permission from the David Dunlap Observatory.

Every photometric system can be calibrated against MK spectral types; for instance, by observing a large number of A0 V stars, it is possible to find mean $b-y$, m_1, and c_1 indices for that spectral type. Tabulations of such mean values can be found in a number of sources, including Drilling & Landolt (1999). Some astronomers have been tempted to reverse the process, i.e., to obtain photometric indices for their stars of interest, and then to "derive" MK spectral types via the tabulations. This practice is deprecated (see, for instance, the comments after the paper by Heck 1984), as an MK type is properly determined only through detailed comparison of the unknown spectrum with the MK standards. As will become evident in the following chapters, the combined effects of rotation, metallicity, interstellar reddening, and other *photometric degeneracies* can confuse the translation of photometric indices into MK types, even if such a translation were

Table 2.2 SDSS filter Effective Wavelengths

u'	g'	r'	i'	z'
3551 Å	4686 Å	6165 Å	7481 Å	8931 Å

desirable or legitimate. Rather, the MK type should be regarded as an independent datum of stellar astronomy, capable of yielding insight and information when confronted with other data types, such as photometry. Some of these issues are considered in more detail by Crawford (1984) and Gray (2006).

That is to say, the most productive relationship between MK classification and multicolor photometry is one of *complementarity*. The complementary nature of the interaction between spectral classification and multicolor photometry comes about because these two systems approach the classification of stars in two very different ways. Multicolor photometric systems, for the most part, are confined to measuring continuum features in a stellar spectrum, such as the slope of the Paschen continuum, the Balmer jump, etc. Spectral classification, on the other hand, relies almost entirely on the appearance of the line spectrum. In most cases, the two systems give consistent classifications, but the most interesting comparisons arise when the two systems *disagree*. In that disagreement is often found new information about stellar atmospheres, stellar evolution, or even the interstellar medium. Thus, one's spectral type for a given star should never be influenced by photometric information, because that influence would rob the interface between the two systems of any information content.

The first, and in some ways still the best, example of complementarity between the two systems is the determination of reddening due to the presence of interstellar dust. Interstellar dust *reddens* the light from a star by preferentially scattering out of the line of sight short wavelength light. Reddening, of course, affects the photometric measurement of the color of the star (for instance, the B–V and $b-y$ indices are made more positive), but has little effect on the line spectrum and thus the spectral type. Therefore, if *intrinsic colors* for the different spectral types are found by studying nearby, unreddened stars, the *color excess*, or *reddening*, for a given star may be determined by comparing the measured color index to the intrinsic color index determined from its spectral type. These color excesses take the form

$$E(B-V) = (B-V) - (B-V)_0 \tag{2.3.1}$$

where $(B$–$V)_0$ is the intrinsic color of the star.

There are many other instances of complementarity between photometry and spectral classification; the history of the Strömgren $uvby\beta$ system is particularly rich in examples. This profitable interaction has been expertly reviewed by Olsen (1994).

2.4 PHYSICAL PRINCIPLES UNDERLYING THE MK SEQUENCE

2.4.1 Physical Conditions in Stellar Photospheres

While a theoretical understanding of the formation of the stellar spectrum is certainly not necessary for the process of spectral classification, it is essential for the *interpretation* of spectral types. It is beyond the scope of this book to develop the theory of stellar atmospheres and spectral-line formation in detail; excellent monographs exist on that subject (i.e., *The Observation and Analysis of Stellar Photospheres*, Gray 2008; and *Stellar Atmospheres*, Mihalas 1978). However, it is possible to gain a physical understanding of the spectral sequence and other aspects of stellar spectral classification by considering some elementary results of statistical physics and radiative transfer.

First, it is necessary to understand that the stellar spectrum is formed only in the surface layers of a star, called the *stellar photosphere*, although in cool stars the chromosphere and the corona also contribute to the emergent spectrum, especially in the far and extreme ultraviolet. The stellar photosphere plays such an important role in the formation of the spectrum because it is here that photons undergo their last few, and thus most critical, interactions with matter before escaping to free space.

Energy in the form of photons, produced in the core of the star by nuclear reactions, reaches the surface of the star only after countless interactions with the material in the interior of the star. The interior of a star is composed of a nearly completely ionized plasma (a gas consisting of electrons and ions). This plasma interacts with the radiation field in the interior through the physical processes of electron scattering and free–free and bound–free (photoionization) absorption and emission by ions. Free–free absorption occurs when a free electron becomes able to absorb a photon when in the vicinity of an ion. Thus a gamma-ray photon produced in the core of the star random walks its way to the surface and, in the process, is degraded into hundreds of lower energy photons (mostly in the UV, optical, and infrared parts of the spectrum). In the interior, because of the high densities, the *mean free path* between interactions is very short—on the order of a centimeter in main-sequence stars. The high densities also mean that in the interior, collisions are extremely effective in coupling the radiation field with the thermal state of the gas. In this condition, the interior is very nearly in a perfect state of thermodynamic equilibrium, and, as a consequence, the material in the interior of the star radiates at the local temperature as a *blackbody radiator*. As we move toward the surface and encounter lower densities, the mean free path of a typical photon becomes much longer. In the stellar photosphere, the mean free path may measure in the kilometers; eventually a level in the stellar photosphere is reached at which it is highly probable that the photon will escape without further interaction. Since at each interaction the energy (wavelength) of the photon may be altered, it is clear that the last few interactions are most important in the formation of the emergent spectrum.

Because the mean free path of a typical photon in the stellar photosphere is quite long, this means that the radiation field is not so tightly coupled to the

local thermal state of the gas, and thus the assumption that the gas is in a state of thermodynamic equilibrium is no longer strictly valid. However, in high-density, high-pressure atmospheres (main-sequence stars), and to a more limited extent in giant and supergiant stars, *local thermodynamic equilibrium*, i.e., the assumption that each layer in the stellar photosphere is characterized thermodynamically and radiatively by the local gas temperature, is an acceptable approximation, at least for the discussion below.

The physical processes of electron scattering and free–free and bound–free absorption by ions are referred to collectively as sources of *continuous opacity*, as these processes can scatter or absorb and emit photons over a wide range of wavelengths. In the stellar atmosphere other forms of opacity come into play. In particular, bound–bound absorption (i.e., absorption in spectral lines, or *line opacity*) is important. As a consequence, opacity in the stellar photosphere is a strong function of wavelength; in the core of a spectral line the opacity is considerably higher than in the surrounding continuum, where the opacity is due only to continuum processes.

There is a temperature gradient in a stellar photosphere; neglecting the possible existence of extended outer layers of the atmosphere—e.g., the corona and the chromosphere—the top (outer layer) of the photosphere is considerably cooler than the "bottom" (inner layer). This temperature gradient is one of the most important factors in the formation of absorption lines in the stellar spectrum. To understand how an absorption line is formed, compare a continuum region of a stellar spectrum with a spectral line. In the continuum region the total opacity is relatively low, as only continuum processes contribute. This means that we can see at those wavelengths deeply into the photosphere to relatively hot layers and thus the emerging radiation flux is high. In the core of a spectral line the opacity is high, and thus the majority of the photons emerge from higher, cooler layers. This leads to a lower radiation flux in the core of the spectral line than in the surrounding continuum, and thus the formation of an absorption line (see Figure 2.11).

The core of an absorption line is therefore formed in the cool upper layers of the stellar photosphere, the surrounding continuum is formed at depth, and the wings of the absorption line in intermediate layers. This implies that if the continuous opacity is relatively high, the spectral line will be formed only over a limited range in the atmosphere, and thus will be weaker than if the continuous opacity were low. This suggests that the strength of a spectral line is in inverse proportion to the continuous opacity and in direct proportion to the line opacity. Factors that contribute to the line opacity include the abundance of the relevant element in the photosphere, the proportion of the atoms that are in the ionization state and the excitation state required for absorption in the spectral line under consideration, and the transition probability associated with the spectral line. If we let κ_λ represent the continuous opacity per unit mass at the wavelength of the spectral line, and l_λ the line opacity, we then have, to a first approximation,

$$\text{Line Strength} \propto \frac{l_\lambda}{\kappa_\lambda}. \tag{2.4.1}$$

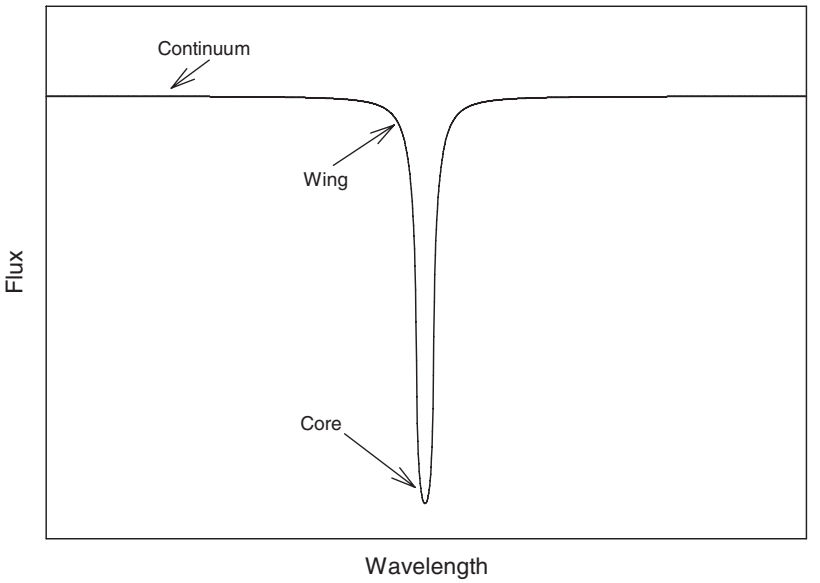

Figure 2.11 The parts of a spectral line.

This relationship is strictly true only for weak spectral lines. For strong lines, effects such as the various line-broadening mechanisms, saturation, and turbulence mean that the line strength will be a nonlinear but monotonically increasing function of l_λ/κ_λ. Details may be found in Gray (2008) and Mihalas (1978).

Figure 2.12 shows, graphically, the continuous opacity at $\lambda = 4500\,\text{Å}$ as a function of the temperature. Some of the important contributers to the continuous opacity are indicated in that figure.

Emission lines, when they are present in stellar spectra, usually, although not always, originate in hotter, outer layers of a stellar atmosphere, such as a chromosphere, a corona, or a stellar wind. These emission lines are usually most evident in regions where the flux in the photospheric spectrum is small, such as the cores of strong absorption lines (the Hα line, for example) and, in cool stars, in the short-wavelength ultraviolet.

An understanding of the physical processes that lead to the formation of the stellar spectrum requires some knowledge of representative temperatures, densities, and pressures in the stellar photosphere. The *effective temperature* (T_{eff}) of a stellar photosphere corresponds, roughly, to the temperature of the layer where the spectral continuum is formed. The T_{eff} of a star is defined to be the temperature of a blackbody radiator with the same radius and the same total power output (luminosity) as the star. Effective temperatures range from about 2500 K at the bottom of the stellar main sequence (late M-type dwarfs, not counting the L and T brown dwarfs) to more than 40,000 K at the top (early O-type stars). With a knowledge of the opacity mechanisms in a stellar photosphere, it is possible to compute a theoretical stellar atmosphere model. Theoretical stellar atmosphere models have been computed for effective temperatures all along the main sequence and these

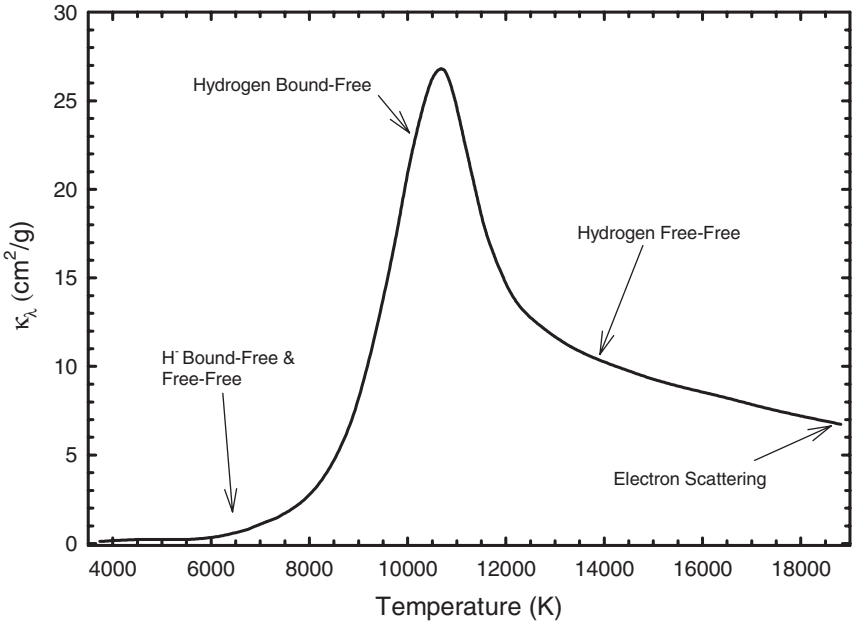

Figure 2.12 Continuous opacity in the optical region (calculated at 4500 Å at unit *optical depth*) in stellar photospheres along the main sequence as a function of the temperature. The dominant sources of opacity are indicated.

models give us information on the temperature structure and the run of densities and pressures with depth in the photospheres of these stars. Models for giants and supergiants have also been computed.

Along the main sequence, typical pressures in stellar photospheres range from very low values at the surface to about a few$\times 10^5$ or 10^6 dynes cm^{-2} at the "bottom" (for the purpose of comparison, the pressure of the earth's atmosphere at sea level is about 10^6 dynes cm^{-2}). Electron number densities are, of course, strongly dependent on the effective temperature, and range from typical values of 10^{12} to 10^{13} cm^{-3} in the late type stars to 10^{14} to 10^{15} cm^{-3} in the early-type stars. These values will be one to two orders of magnitude smaller in the giants, and another one to two orders of magnitude smaller in the supergiants.

2.4.2 The Hydrogen Lines

Let us now use our understanding of spectral-line formation in stellar atmospheres to understand, in physical terms, the broad outline of the spectral sequence. In §2.2 we saw that one of the outstanding features of the spectral sequence is the behavior of the hydrogen lines. In the late-type stars, the hydrogen lines are weak, but become steadily stronger with increasing effective temperature until reaching a maximum in the early A-type stars. At higher temperatures (the B- and O-type stars), the hydrogen lines again become weaker. We saw this behavior in the Balmer lines of hydrogen in main-sequence (Figure 2.2) and supergiant (Figure 2.4) stars and in

the Brackett lines in main-sequence stars (Figure 2.7). We noted, however, that in the supergiants the Balmer lines come to a maximum at a later spectral type than in the main-sequence stars, and the Brackett lines in main-sequence stars come to a maximum at slightly earlier spectral types than the Balmer lines. What are the physical principles underlying this behavior?

The behavior of the Balmer lines in the main-sequence stars may be understood qualitatively as follows. The Balmer series of absorption lines arises from transitions out of the first excited state ($n = 2$) of the hydrogen atom, where n is the principal quantum number of the hydrogen atom. In the late-type stars the photospheric temperatures are low enough that only a very small proportion of the hydrogen atoms have been excited to the $n = 2$ state; most are in the ground ($n = 1$) state. As we move toward earlier types, the photospheric temperatures rise, and a greater proportion of the hydrogen atoms are in the $n = 2$ state. This leads to an increase in the line opacity, l_λ, and the Balmer lines increase in strength. At yet higher temperatures (earlier types), hydrogen begins to become ionized, and so while the proportion of neutral hydrogen atoms in the $n = 2$ state is still increasing, the actual number of atoms in that state is actually declining. This leads to a decline in the line opacity, and a weakening of the Balmer lines. As we shall see later, the continuous opacity plays only a relatively minor role in determining the behavior of the Balmer lines near their maximum.

We can discuss the behavior of the hydrogen lines in a more quantitative way by considering two important equations of statistical physics. The first of these equations is the Boltzmann equation, which is strictly valid only in the condition of thermodynamic equilibrium. The Boltzmann equation relates the number densities of a given species (atom or ion) in two different excitation states:

$$\frac{N_B}{N_A} = \left(\frac{g_B}{g_A}\right) \exp[(E_A - E_B)/kT] \tag{2.4.2}$$

where N_A and N_B are the number densities of the particular species in the two different excitation states, A and B; E_A and E_B are the excitation energies of those two states, k is the Boltzmann constant, T is the temperature, and g_A and g_B are the statistical weights of the levels A and B (for hydrogen, $g_n = 2n^2$). We can write the ratio $N_n/N_{(0)}$, where N_n is the number density of hydrogen atoms in the nth state and $N_{(0)}$ is the total number density of neutral hydrogen atoms, as

$$\begin{aligned}\frac{N_n}{N_{(0)}} &= \frac{N_n}{N_1 + N_2 + N_3 + \cdots} = \frac{N_n/N_1}{[1 + N_2/N_1 + N_3/N_1 + \cdots]} \\ &= \frac{g_n \exp(-E_n/kT)}{[g_1 + g_2 \exp(-E_2/kT) + g_3 \exp(-E_3/kT) + \cdots]} \\ &= \frac{g_n \exp(-E_n/kT)}{U(T)}\end{aligned} \tag{2.4.3}$$

where $U(T)$ is the partition function for neutral hydrogen. It is defined as

$$U(T) = \sum g_i \exp(-E_i/kT) \tag{2.4.4}$$

where the sum is over all bound states in the hydrogen atom. For $T \lesssim 20{,}000\,\mathrm{K}$, $U(T)$ varies between 2.0 and ≈2.5.

The second equation is the Saha equation, again strictly valid only under conditions of thermodynamic equilibrium. The Saha equation relates the number densities of ions in two adjacent ionization states, $N_{(i+1)}$ and $N_{(i)}$:

$$\frac{N_{(i+1)}}{N_{(i)}} = \frac{U_{(i+1)}}{U_{(i)}} \frac{1}{N_e} \frac{2(2\pi mkT)^{3/2}}{h^3} \exp(-E_I/kT) \tag{2.4.5}$$

where E_I is the ionization energy of the ith ion, N_e is the electron number density, m is the electron mass, and $U_{(i+1)}$ and $U_{(i)}$ are the partition functions of the two ionization states. There are only two ionization states for hydrogen: neutral hydrogen and hydrogen that has lost its single electron, i.e. a proton. It turns out that the partition function for a proton, U_p, is identically 1.0. We may therefore write

$$\frac{N_p}{N_{(0)}} = \frac{1}{U(T)} \frac{1}{N_e} \frac{2(2\pi mkT)^{3/2}}{h^3} \exp(-E_I/kT). \tag{2.4.6}$$

Now, according to our discussion in the paragraphs above, the line opacity, l_λ, for a hydrogen line arising from the nth energy level should be proportional to the ratio of the number density of neutral hydrogen atoms in the nth excitation state, N_n, to the total number density of hydrogen, $N_{(0)} + N_p$. Thus for a hydrogen line, we may write

$$l_\lambda \propto \frac{N_n}{N_{(0)} + N_p} = \frac{N_n/N_{(0)}}{N_p/N_{(0)} + 1}. \tag{2.4.7}$$

Substituting from Equations 2.4.3 and 2.4.6, and simplifying we find

$$l_\lambda \propto \frac{N_n}{N_{\mathrm{total}}} = \frac{g_n N_e h^3 \exp(-E_n/kT)}{2(2\pi mkT)^{3/2} \exp(-E_I/kT) + N_e h^3 U(T)}. \tag{2.4.8}$$

What about the continuous opacity? Figure 2.12 shows that the continuous opacity in the vicinity of the Balmer lines peaks strongly at a temperature of about 11,000 K. However, it turns out that the variation in the hydrogen line opacity with temperature is many orders of magnitude greater than the variation in the continuous opacity. Thus, we may safely ignore the effects of the continuous opacity in this calculation, although it must, of course, be taken fully into account in detailed spectral synthesis computations.

Thus, a plot of the quantity N_n/N_{total} given by the equation above versus temperature should mirror the behavior of the hydrogen lines. For the Balmer lines in main-sequence stars, we substitute $n = 2$, $E_2 = 10.2\,\mathrm{eV}$, $E_I = 13.6\,\mathrm{eV}$, and $N_e = 1.0 \times 10^{14}\ \mathrm{cm}^{-3}$, a typical value for a main-sequence stellar atmosphere near the Balmer maximum.[3] The result is shown as the solid line in Figure 2.13. Notice how this curve peaks near T =10,000 K, which is approximately the temperature

[3] One electron volt (eV) is the energy acquired by an electron when it is accelerated through a potential difference of one volt, and is equal to 1.602×10^{-19} joule or 1.602×10^{-12} erg.

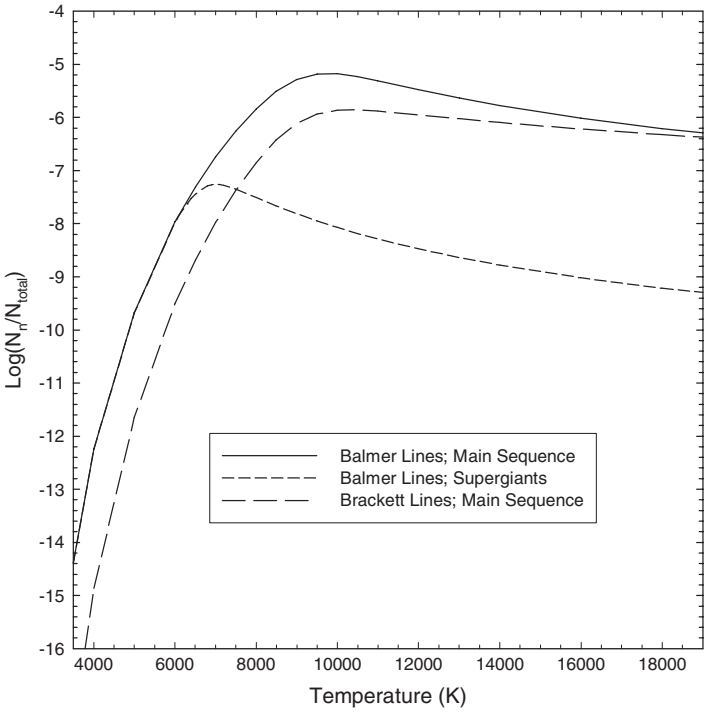

Figure 2.13 Behavior of the hydrogen lines with temperature.

of an A0 star. In main-sequence stars, the actual peak is near 9000 K, but this discrepancy is easily explained by our neglect of a number of more subtle physical effects that can be taken into account only through a full stellar-atmosphere and radiative-transfer treatment. If we use a value of the electron number density more typical of Ib supergiants, say, $N_e = 1.0 \times 10^{11}\,\mathrm{cm}^{-3}$, we get the short-dashed curve. Note that this peak is at a significantly cooler temperature, about 7000 K, very close to the maximum near spectral type F0 we observed in Figure 2.4. Finally, again using $N_e = 1.0 \times 10^{14}\,\mathrm{cm}^{-3}$, but this time $n = 4$, $E_4 = 12.75\,\mathrm{eV}$, appropriate numbers for the Brackett series of hydrogen lines in main-sequence stars, we obtain the long-dashed curve. Notice that the maximum is at a slightly higher temperature than for the main-sequence Balmer lines, exactly as we observed earlier in this chapter.

A very similar analysis may be carried out for the neutral helium lines; the only difference is that we would have to consider three ionization states (He I, He II, He III) instead of two. Considering that the excitation energies for He I lines in the optical are considerably higher than for the hydrogen lines, and the ionization energy for He I is also higher, it is easy to understand why the maximum for the He I lines occurs at about 22,000 K, instead of 10,000 K.

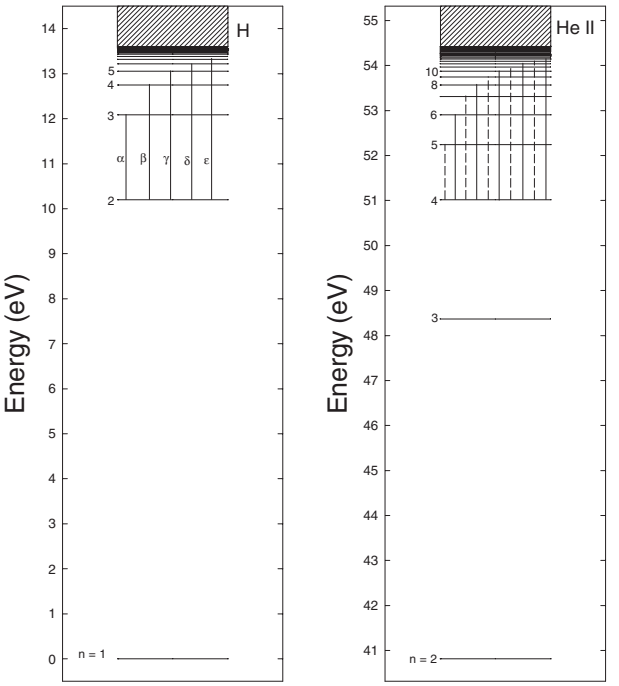

Figure 2.14 Simplified energy-level diagrams for hydrogen (left) and ionized helium (right). The principal quantum numbers for the energy levels are indicated in both panels; $n = 1$ is the ground state. Note that the ground state of He II is not shown in the diagram. In the panel to the left, transitions corresponding to the first few lines of the hydrogen Balmer series are shown. On the right, transitions corresponding to the Pickering series of He II are shown. Note that every other Pickering line (solid lines) corresponds closely in energy to a line of the Balmer series. The hatched area in both diagrams represents the continuum of the two ions.

2.4.3 He II lines

Lines of He II show up in hot stars, not only in the O-type stars (Chapter 3), but also in the Wolf–Rayet stars (Chapter 11). In those chapters, frequent reference is made to the Pickering series of He II, and how it relates to the Balmer series of hydrogen. Ionized helium and neutral hydrogen are one-electron systems, and thus have similar energy-level diagrams, except that the energies for He II are scaled by a factor of Z^2 compared with those for hydrogen, where Z refers to the nuclear charge. Since $Z = 1$ for hydrogen, and $Z = 2$ for He II, the scaling is by a factor of 4. Figure 2.14 shows the energy-level diagrams for hydrogen and He II. In the diagram for hydrogen, transitions corresponding to the first few lines of the Balmer series are shown. In the diagram for He II, transitions corresponding to the Pickering series are shown. Note that the $2 \rightarrow 3$ transition in hydrogen corresponds very closely in energy to the $4 \rightarrow 6$ transition for He II, similarly for the $2 \rightarrow 4$ transition of hydrogen and the $4 \rightarrow 8$ transition for He II and so on. What this

means is that every other line of the Pickering series corresponds very closely in wavelength to a line of the Balmer series. Similar overlaps may be seen in other series. For instance, the Lyman series of hydrogen ($1 \rightarrow m$) overlaps with every other line of the Balmer series of He II ($2 \rightarrow m$). The Paschen series of He II ($3 \rightarrow m$) has one line in the optical, λ4686 ($3 \rightarrow 4$), which figures prominently in the classification of the Wolf–Rayet stars.

2.4.4 The Metallic Lines

The behavior of the spectral lines due to metals, which we described in §2.2, obey the same general principles as the hydrogen lines (see §2.4.2). However, careful consideration of Figure 2.15, a temperature sequence of main-sequence stars in the blue-violet region, shows some aspects of this behavior that are not immediately understandable. For instance, the enormous strength of the Ca II K & H lines compared with lines of Fe II is somewhat puzzling considering that iron is nearly 10 times more abundant than calcium in a typical stellar photosphere. Likewise, titanium is about 2.5 orders of magnitude less abundant than iron, and yet Ti II lines in the A5 V star in that figure are of comparable strength to the Fe II lines. The almost complete lack of strong metal lines in the B-type stars also seems curious. For instance, we might expect many strong lines of Fe III or Fe IV in the spectrum of a B3 V star, but none show up in Figure 2.15. The explosive growth of Ca I λ4226 toward later types is also notable, and needs further explanation.

2.4.4.1 Resonance Lines

While most spectral lines of metals follow the same pattern of behavior as the hydrogen lines, that is, they come to a maximum at some intermediate temperature depending upon the excitation energy and the ionization energy, *permitted* lines that arise from the ground state of the atom or ion (called *resonance lines*, see Figure 2.16) are an exception. At low temperatures, atoms and ions are preferentially found in the ground state, and hence the strength of these lines, in particular the resonance lines of neutral species, grows dramatically with declining temperature. This is exactly the behavior we noted in the 4226 Å resonance line for Ca I. The resonance lines of ions also tend to grow fairly dramatically with decreasing temperature, but this growth is reversed at temperatures low enough that the ion in question is no longer the dominant ionization state. For instance, the Ca II K & H lines, both resonance lines for the Ca II ion, grow with decreasing temperatures down to a spectral type of about K5 ($\approx$4500 K) on the main sequence, and then fade rapidly after that. The reason for this is that Ca I is transitioning to the dominant ionization state in the spectral line–forming region in stellar photospheres on the main sequence for $T_{\rm eff} \lesssim 4500$ K. This fact also helps to explain the explosive growth of the Ca I resonance line in spectra later than about K5.

It stands to reason, therefore, that the resonance lines for a given atom or ion will usually figure prominently among the strongest lines of that species in a stellar spectrum. It turns out, however, that for many species the resonance lines are

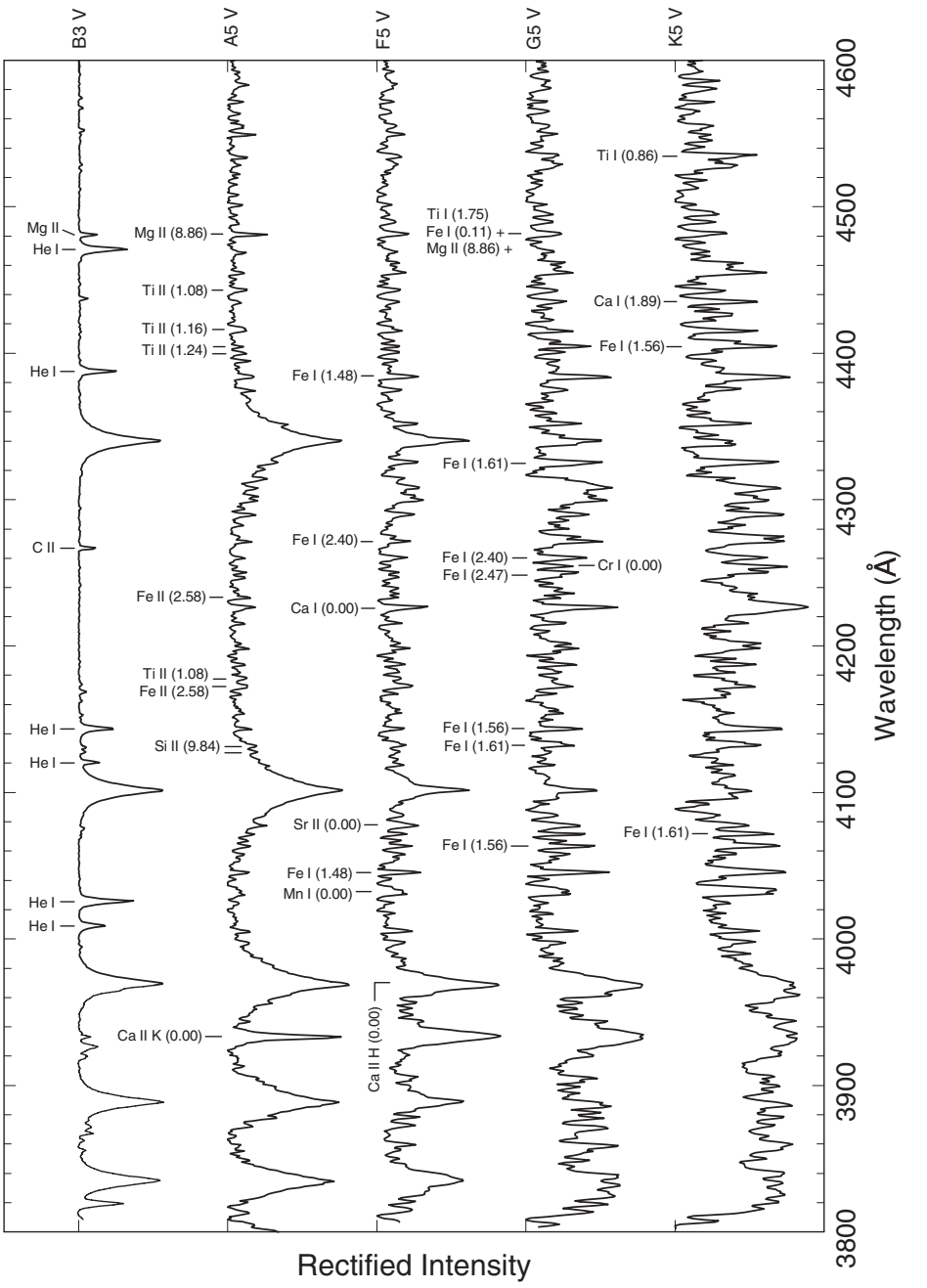

Figure 2.15 Main Sequence stars B3–K5 with a resolution of 1.8 Å. Many of the strongest lines in these spectra are identified. The numbers in parentheses indicate the excitation energy in electron volts (eV) of the lower state for these transitions. These spectra have been rectified and offset vertically by 0.7 continuum units.

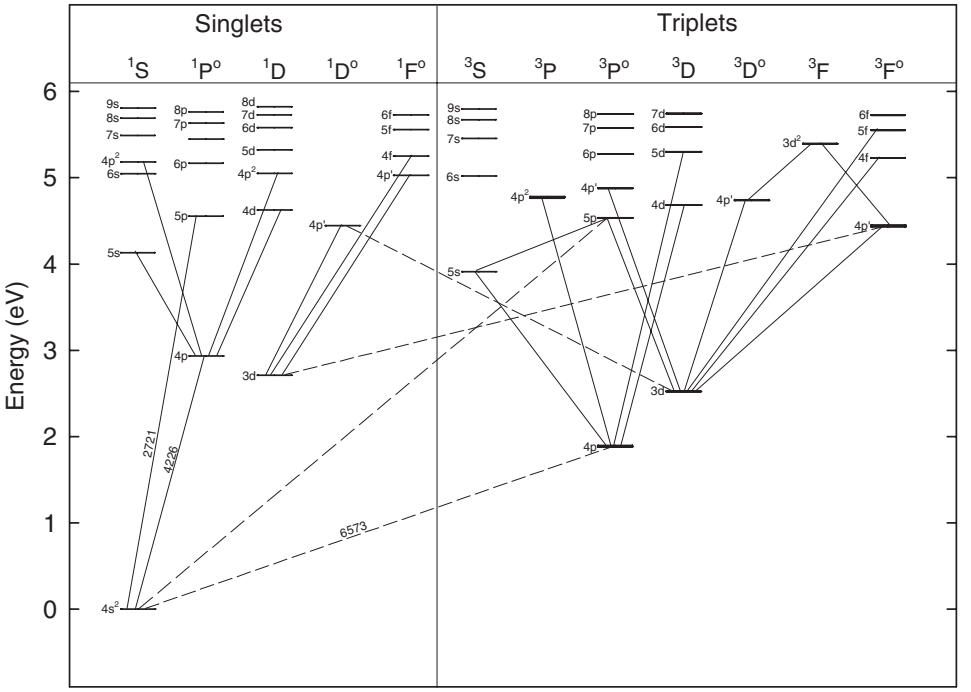

Figure 2.16 A simplified energy-level (Grotrian) diagram for Ca I. A number of important permitted transitions are indicated (solid lines) including two resonance lines, λλ2721 and 4226, as well as some intercombination lines (dashed lines) including λ6573.

in the ultraviolet and not in the optical, and thus do not appear in the traditional blue-violet classification region. For instance, the resonance lines of hydrogen—the lines of the Lyman series—lie in the ultraviolet; Lyα has a wavelength of 1216 Å. The resonance lines of He I are in the far UV; the longest wavelength resonance line of He I is at 584 Å. As a very rough rule of thumb, the energy of the first excited state in a given species scales with the ionization energy and thus the wavelength of the longest wavelength resonance line of a given species will vary inversely with the ionization energy of that species. That means that species with high ionization energies will have their resonance lines in the UV, whereas resonance lines in the optical belong to species with relatively low ionization energies. As an example, neutral sodium has a relatively low ionization energy of 5.1 eV and its longest wavelength resonance lines, the sodium D-lines, have wavelengths of about 5890 Å, in the yellow. Table 2.3 lists the wavelengths of the longest wavelength prominent resonance line along with the ionization energy (I.P.) in electron volts for a number of important species.

It is important to understand, however, that not all lines that arise from the ground level are resonance lines or are particularly strong. For instance, the Ca I λ6573 line arises from the ground state, but is not a resonance line (see Figure 2.16). This line is an example of an *intercombination line*, in that the upper

Table 2.3 Longest Wavelength Resonance Lines and Ionization Potentials

Ion	λ_{RL}(Å)	I.P.(eV)	Ion	λ_{RL}(Å)	I.P.(eV)
H I	1216	13.6	He II	304	54.4
He I	584	24.6	C II	1335	24.4
C I	1657	11.2	C III	977	47.9
Na I	5890	5.1	Mg II	2802	15.0
Mg I	2852	7.6	Ca II	3968	11.9
Ca I	4226	6.1	Ti II	3383	13.6
Ti I	5173	6.8	Fe II	2599	16.2
Fe I	3860	7.9	Fe III	1123	30.7

level is a triplet state ($^3P_1$ with a total electronic spin $S = 1$),[4] and the lower state, the ground state, is a singlet ($^1S_0$ with a total electronic spin $S = 0$). This transition violates the quantum mechanical *selection rule* $\Delta S = 0$, which states that the total electronic spin should not change during a radiative transition.[5] As a consequence, Ca I λ6573 has a relatively low *transition probability*, and thus is an inconspicuous line. Another quantum mechanical selection rule involves the angular momentum quantum number, l. Transitions that violate $\Delta l = \pm 1$ are called *forbidden lines* and are almost always very weak in stellar spectra. They can, however, be quite strong under low-density conditions (see, for examples, §4.6.1 and §12.3.1). On the other hand, the Ca I λ4226 line arises from the ground state and obeys both of these selection rules. It thus has a high transition probability, and is one of the strongest lines of Ca I in a stellar spectrum.

2.4.4.2 Excitation and Ionization

In the spectrum of Fe II, the longest wavelength resonance line is located at 2599 Å in the ultraviolet. What this means is that all prominent Fe II lines in the optical region arise from excited states (see Figure 2.17). Lines that arise from excited states are weakened by an additional factor, the Boltzmann factor, relative to the resonance lines, which governs the population of the lower state of the transition:

$$g_i \exp(-E_i/kT)$$

where g_i is the statistical weight of the lower level, and E_i is the excitation energy.

Figures 2.15 and 2.17 help to explain why lines of Fe II are of comparable strength to Ti II lines in the traditional spectral classification region (3800–5000 Å) in the A-type stars even though iron is 2.5 orders of magnitude more abundant than titanium: note that the strongest Fe II lines in this region have excitation energies that are considerably larger than those of the strongest Ti II lines. The difference in the Boltzmann factors partially cancels the difference in the abundances. Of course, there is another factor that is important here: the ionization energy of Ti I

[4]The *multiplicity* of the term is given by $2S + 1$.

[5]The selection rule $\Delta S = 0$ is strictly valid only under the condition of pure *LS* coupling. The *LS* coupling scheme breaks down for the heavier elements, and so *intercombination lines* can be stronger for those elements. See the Glossary for further details.

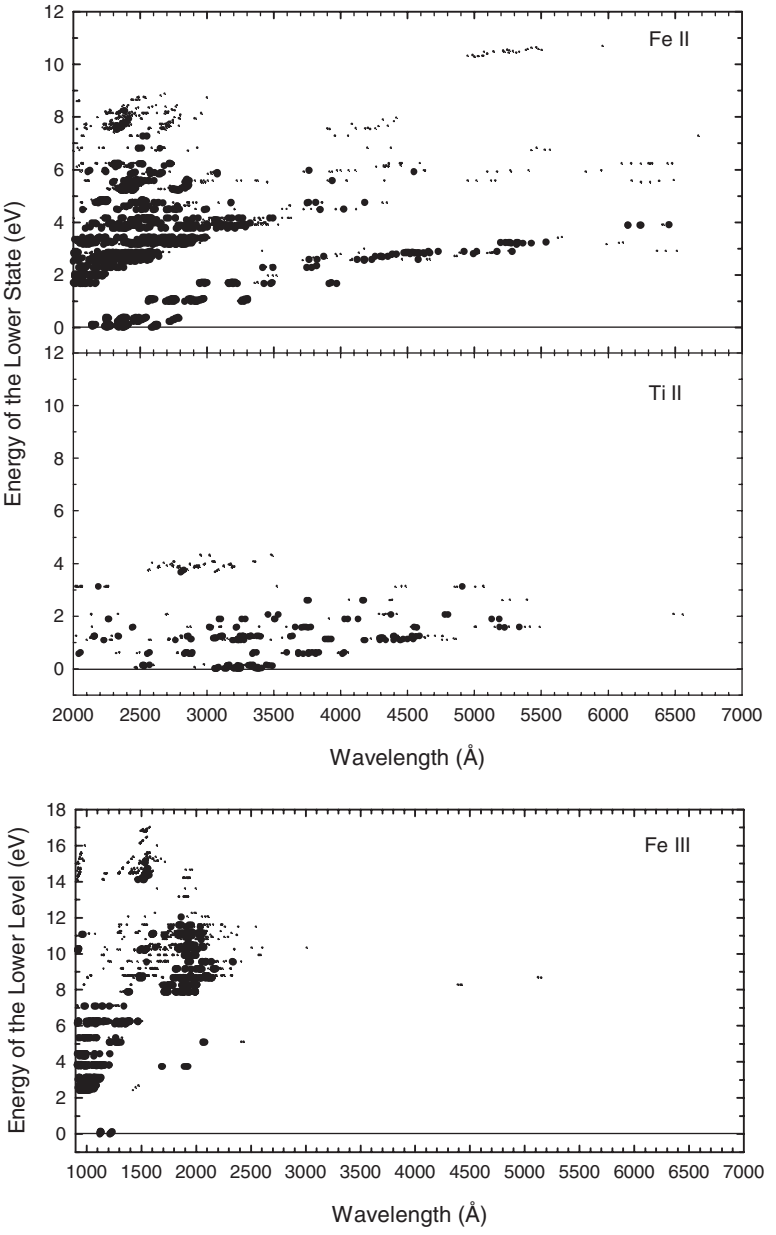

Figure 2.17 Excitation energy of the lower level for spectral lines with *equivalent widths* (W_λ) greater than 10 mÅ of Fe II, Ti II, and Fe III as a function of wavelength. The filled circles represent strong spectral lines ($W_\lambda > 50$ mÅ), the dots represent weaker spectral lines. The horizontal line at $E = 0$ eV in each plot represents the energy of the ground state. The line strengths were calculated using the stellar spectral synthesis program SPECTRUM using Kurucz (1993) stellar atmosphere models. A model with an effective temperature of 8500 K (representative of A-type stars) was used for the Fe II and Ti II calculations, and a model with an effective temperature of 15,000 K (representative of B-type stars) was used for the Fe III calculations.

Table 2.4 Energy, Wavelength and Temperature Equivalents

Energy	1 eV	3 eV	3.4 eV	8 eV	10.2 eV	13.6 eV
$\lambda = hc/E = hc/(kT)$	12398 Å	4133 Å	3647 Å	1550 Å	1216 Å	912 Å
$T = E/k$	11605 K	34814 K	39455 K	92836 K	118366 K	157821 K

is significantly lower than that of Fe I (see Table 2.3), and thus the ionization of titanium is more advanced than that of iron, increasing the abundance of Ti II relative to Fe II.

Notice that the plots in Figure 2.17 for Fe II and for Ti II are quite similar except (1) the range of energies for the lower state of the spectral lines of Ti II is compressed relative to that of Fe II, and (2) the resonance lines of Ti II extend to considerably longer wavelengths than do those of Fe II. Both of these effects can be understood qualitatively on the basis of the scaling of the energy levels of a given ion by the ionization energy.

The Fe II and Ti II lines in the blue-violet region of the spectrum that arise from relatively low-lying excited states play a very special role in spectral classification. These are the strong lines that lie on the lower envelopes of the distributions in the top two panels in Figure 2.17. The lower levels of these lines are classified as *metastable states*, which means, in this context, that a radiative transition between one of these states and any lower level including the ground state would be forbidden as it would violate the selection rule $\Delta l = \pm 1$. As a consequence, in low-density, low-pressure environments (such as the atmospheres of supergiants) where collisions are less important, these states will have higher populations than indicated by the Boltzmann equation. This leads to an enhancement of these lines in supergiant A- and F-type stars (compare Figure 2.4 with Figure 2.2), making them useful in luminosity classification (see §2.2.4). We will discuss these lines in much more detail in Chapter 6 on the F-type stars.

The lack of strong lines of Fe III in the blue-violet region of the spectrum of B-type stars is readily understood on the basis of the lower panel in Figure 2.17. Note that the longest wavelength resonance lines of Fe III lie in the far ultraviolet, and that the few weak lines that do show up in the blue-violet have excitation energies on the order of 8–9 eV. However, this same plot suggests that the ultraviolet region of B-type stars should be richly populated with lines of Fe III, and indeed this is the case. Note as well that the ultraviolet region of A-type stars (top two panels in Figure 2.17) has a high density of Fe II lines. Indeed, the line absorption is so great in this region that the ultraviolet flux is strongly attenuated in the A-type stars (see Figure 2.6).

Table 2.4 is included for the convenience of the reader, and gives energy equivalents in terms of wavelengths and kelvins. For instance, a photon with an energy of 1 eV has a (vacuum) wavelength of 12398 Å (1.2398 μm). A 13.6-eV photon with a wavelength of 912 Å is just able to photoionize a hydrogen atom in the ground state, and a 3.4-eV photon with a wavelength of 3647 Å is just able to photoionize a hydrogen atom in the first excited state ($n = 2$); this corresponds to the

wavelength of the Balmer jump. The factor kT, where k is the Boltzmann constant (8.617×10^{-5} eV/K), is found in many of the equations of statistical physics (including the Boltzmann equation, Eq. 2.4.2 and the Saha equation, Eq. 2.4.5) and has the units of energy. This factor may be used to define a temperature equivalent of the energy ($T = E/k$), which has a number of uses. For instance, if an energy level has an excitation energy of 1 eV, then, according to the Boltzmann equation, the population of that state will be comparable to the population of the ground state at the equivalent temperature of 11605 K. Note from the table that the temperature equivalent of 10.2 eV—the excitation energy of the first excited state in hydrogen, is 118366 K—which implies that at normal photospheric temperatures in stars, the population of the first excited state of hydrogen is a tiny fraction of that of the ground state.

2.4.4.3 The Continuous Opacity

One final factor is important in the behavior of the metallic lines in stellar spectra. Note that in the optical the overall strength of the metallic-line spectrum declines sharply with increasing temperature as we move from the K-type stars to the A-type stars. While individual lines will grow and decline in strength as a function of the temperature, according to the principles we have discussed above, this general decline in the strength of the metallic lines is due, in part, to the effect of the continuous opacity. Recall that the line strength is, at least to a first-order approximation, inversely proportional to the strength of the continuous opacity (see Equation 2.4.1). Figure 2.12 shows how this continuous opacity changes with temperature in the optical region of the spectrum. The steep rise in this continuous opacity to a sharp peak at about 11,000 K (the effective temperature of the late B-type stars) is important in the decline of the metallic-line strengths. But should we not, then, expect a rise in the strength of the metallic lines in the B-type stars to coincide with the decline in the continuous opacity with increasing temperature? The answer is that in the B-type stars, the most abundant metals (iron, calcium, etc.) exist predominately in the second (III) or even third (IV) ionization states. We have already seen that in the optical these ions exhibit only very weak lines in stellar spectra. However, in the ultraviolet, the B-type stars do have very rich metallic-line spectra.

Bibliography

Canterna, R. 1976, AJ, 81, 228
Crawford, D.L. 1975, AJ, 80, 955
Crawford, D.L. 1978, AJ, 83, 48
Crawford, D.L. 1979, AJ, 84, 1858
Crawford, D.L. 1984, in *The MK Process and Stellar Classification*, ed. R.F. Garrison (David Dunlap Observatory: University of Toronto), p. 191
Crawford, D.L., & Mander, J. 1966, AJ, 71, 114
Drilling, J.S., & Landolt, A.U. 1999, in *Allen's Astrophysical Quantities*, 4th edition, ed. A.N. Cox (New York: Springer Verlag), p. 381
Gray, D.F. 2008, *The Observation and Analysis of Stellar Photospheres*, 3rd edition (Cambridge: Cambridge University Press)
Gray, R.O. 2006, *Memorie della Società Astronomica Italiana*, 77, 1123
Hearnshaw, J.B. 2005, *The Measurement of Starlight: Two Centuries of Astronomical Photometry* (Cambridge: Cambridge University Press)
Heck, A. 1984, in *The MK Process and Stellar Classification*, ed. R.F. Garrison (David Dunlap Observatory: University of Toronto), p. 222
Johnson, H.L., & Morgan, W.W. 1953, ApJ, 117, 313
Kurucz, R.L. 1993, CD-Rom 13, ATLAS9 Stellar Atmosphere Programs and 2km/s Grid (Cambridge=SAO)
Landolt, A.U. 1992, AJ, 104, 340
McClure, R.D. 1976, AJ, 81, 182
Meyer, M.R., Edwards, S., Hinkle, K.H., & Strom, S.E. 1998, ApJ, 508, 397
Mihalas, D. 1978, *Stellar Atmospheres*, 2nd edition (New York: W.H. Freeman)
Nicolet, B. 1996, *Baltic Astronomy*, 5, 417
Olsen, E.H. 1983, AApS, 54, 55
Olsen, E.H. 1994, in *The MK Process at 50 Years: A Powerful Tool for Astrophysical Insight*, eds. C.J. Corbally, R.O. Gray, & R.F. Garrison, Astronomical Society of the Pacific Conference Series, Vol. 60 (San Francisco: Astronomical Society of the Pacific), p. 119
Olsen, E.H., & Perry, C.L. 1984, AApS, 56, 229
Olsen, E.H. 1995, AA, 295, 710
Skrutskie, M.F., et al. 2006, AJ, 131, 1163
Straižys, V., Crawford, D.L., & Philip, A.G.D. 1996, *Baltic Astronomy*, 5, 83
Strömgren, B. 1966, ARAA, 4, 433
Valdes, F., Gupta, R., Rose, J.A., Singh, H.P., & Bell, D.J. 2004, ApJS, 152, 251
White, N.M., & Wing, R.F. 1978, ApJ, 222, 209